INFLUENCE OF NANOPARTİCLE ADDITION TO ELECTRICAL PROPERTIES OF TCO FILMS PRODUCED USING ELECTROSPINNING TECHNIQUE

BURAK ÇELİK

MAY 2024

ÇANKAYA UNIVERSITY

GRADUATE SCHOOL OF NATURAL AND APPLIED SCIENCES

DEPARTMENT OF MATERIALS SCIENCE AND ENGINEERING

M.Sc. Thesis in

MICRO AND NANO TECHNOLOGY

INFLUENCE OF NANOPARTİCLE ADDITION TO ELECTRICAL PROPERTIES OF TCO FILMS PRODUCED USING ELECTROSPINNING TECHNIQUE

BURAK ÇELİK

MAY 2024

ABSTRACT

Influence of Nanoparticle Addition to Electrical Properties of TCO Films Produced Using Electrospinning Technique

ÇELİK, BURAK

M.Sc. in Micro and Nanotechnology

Supervisor: Prof. Dr. Ziya ESEN

Co-Supervisor: Assist. Prof. Dr. Nilufer DUYGULU

May 2024, 83 pages

In this study, the effect of nanoparticle addition on morphology and electrical properties electrospun nanofibers coated on transparent conductive oxide glass, namely, Indium Tin Oxide (ITO) has been investigated. For this purpose, an aqueous solution of Polyvinyl Alcohol (PVA) was prepared and nanoparticles of silver, zinc oxide, and titanium dioxide were added in the range of 3, 5, 10 and 20 wt.% under the magnetic stirring action. Then, prepared nanoparticle doped PVA solutions were electrospun and coated on ITO glass for 1 h. Morhological characteristics of nanoparticle containing fibers in films were investigated using scanning electron microscope and the resistance and resistivity values of obtained thin films were measured.

It has been observed that the nanoparticles displayed agglomeration in PVA fibers and the size of the agglomerated regions increased as the content of nanoparticle in solution increased. The smallest size of the agglomerated region in all type of solutions was seen in TiO_2 added fibers. As low as 643.7 ± 85.5 nm agglomerate size was detected in 3 wt.% TiO_2 added PVA solutions. Likewise, the smallest fiber diameter size and more homogenous fiber size distribution was observed in TiO_2 added fibers. For example, the average fiber diameter were found to be around 370, 376 and

380 nm for TiO_2, ZnO and Ag nanoparticle doped fibers by 3 wt.%, respectively. Less agglomeration and homogenous fiber size distribution in TiO_2 doped fibers influencedthe electrical conductivity of thin film deposited on ITO glasses positively as well. In all of the thin films containing fibers doped with different amounts of nanoparticles, the resistance and the resistivity values decreased by decreasing the content of nanoparticles. For the TiO_2 doped fiber containing film, the resistance became equilivalent to resistance of ITO glass (34 Ω) at 10 wt.% TiO_2 addition, below which the resistance of the thin film decreased well beyond the resistance of ITO glass as targeted. On the other hand, for the thin films containing fiber doped with ZnO and Ag nanoparticles, ITO resistance value was reached when the nanoparticle content decreased down to 5 wt.%.

Keywords: Electrospinning, Polyvinyl Alcohol, Silver, Zinc Oxide, Titanium Dioxide, Scanning Electron Microscope

ÖZET

Elektro Eğirme Tekniği ile Elde Edilmiş TCO İnce Filmlerde Nanoparçacık İlavesinin Elektriksel Özelliklere Etkisi

ÇELİK, BURAK
Mikro ve Nanoteknoloji Yüksek Lisans

Danışman: Prof. Dr. Ziya ESEN
Ortak Danışman: Dr. Öğretim Üyesi Nilufer DUYGULU
Mayıs 2024, 83 sayfa

Bu çalışmada elektro eğirme yöntemiyle üretilen ve saydam iletken oksit bir cam olan indiyum kalay oksitin (ITO) yüzeyine kaplananan fiberlerde nano parçacık katkılamanın fiberlerin yapısı ve elde edilen ince film elektrik özelliklerine etkisi araştırılmıştır. Bu amaçla, Polivinil Alkol (PVA) sulu çözeltisi hazırlanmış ve manyetik karıştırma yöntemiyle ağırlıkça % 3, 5, 10 and 20 oranında gümüş, çinko oksit ve titanyum oksit katkılaması yapılmıştır. Daha sonra nanoparçacık takviye edilmiş PVA çözeltileri ITO camın üstüne bir saat süreyle elektro eğirme yöntemiyle kaplanlanmıştır. Elde edilen filmlerdeki nanoparçacık takviyeli fiberlerin yapıları taramalı electron mikroskobu ile incelenmiş ve elde edilen ince fimlerin direnç ve özdirençleri değerleri belirlenmiştir.

PVA fiberlerin içinde bulunan nano parçacıkların topaklandığı ve topaklanan bölgelerin büyüklüğünün kullanılan çözelti içindeki nanoparçacık miktarının artmasıyla birlikte arttığı görülmüştür. En az topaklanma TiO_2 takviyeli fiberlerde görülmüş olup, en düşük topaklanma büyüklüğü olan 643.7 ± 85.5 nm ağırlıkça %3 TiO_2 eklenen fiberlerde tespit edilmiştir. Benzer şekilde, en küçük fiber çapı ve homojen fiber büyüklük dağılımı TiO_2 katkılı fiberlerde görülmüştür.

Örneğin, ağırlıkça %3 TiO_2, ZnO ve Ag nanoparçacık içeren fiberlerde fiber çapları sırasıyla 370, 376 and 380 nm olarak ölçülmüştür.

TiO_2 katkılı fiberlerdeki daha az topaklanma ve homojen fiber büyüklük dağılımı ITO cam üzerinde oluşturulan ince filmin elektriksel iletkenliğini de olumlu yönde etkilemiştir. Farklı miktarda nanoparçacık içeren tüm filmlerde nanoparçacık miktarının düşüşüyle birlikte film direnç ve özdirenci de düşmüştür. TiO_2 içeren ince filmlerde, film direnci ITO camın direncine (34 Ω) nanoparçacık takviyesi ağırlıkça %10'a düşürüldüğünde ulaşmıştır ve daha az miktarda TiO_2 ince filmler hedeflendiği şekilde ITO cama göre daha düşük direnç sergilemişlerdir. Diğer yandan, ZnO ve Ag takviyeli ince filmlerde ITO cam direncine ancak nanoparçacık miktarı ağırlıkça %5'e düşürüldüğünde ulaşılabilmiştir.

Anahtar Kelimeler: Elektro Eğirme, Polivinil Alkol, Gümüş, Çinko Oksit, Titanium Dioksit, Taramalı Elektron Mikroskobu

ACKNOWLEDGEMENT

In my thesis study, I am deeply grateful to my mentors, Prof. Dr. Ziya ESEN, who provided me with guidance and unwavering support throughout my academic journey, and Dr. Nilüfer DUYGULU, who generously allowed me to use her laboratory for experimental work and taught me how to operate the equipment used in the experiments. Their invaluable contributions have been instrumental in the successful completion of this research, and for that, I am sincerely thankful.

I express my deepest gratitude to my beloved mother, Behire ÇELİK, my dear father, Ethem ÇELİK and my little sister Intern Dr. Büşra Ecem ÇELİK for their constant love, trust, and unwavering support. Their financial and emotional assistance, as well as their sacrifices, have been instrumental in bringing me to where I am today. With infinite love and respect, I thank them from the bottom of my heart.

TABLE OF CONTENTS

LIST OF TABLE

LIST OF FIGURES

LIST OF SYMBOLS AND ABBREVIATIONS

SYMBOLS

°C	: Celcius
Ω	: ohm

ABBREVIATIONS

cm	: Centimetre
DMF	: Dimetilformamid
TiO_2	: Titaniumdioxide
nm	: nanometer
mm	: millimeter
Ag	: Silver
ZnO	: Zinc oxide
ITO	: Indium Tin Oxide
PVA	: Polyvinyl alcohol
gr	: gram
rpm	: Revolutions per Minute
kV	: kilovolt
mL	: milliliter
DH	: degrees of hydrolysis

CHAPTER I
INTRODUCTION

Energy consumption in the world is rapidly increasing due to population growth, industrialization, and technological advancements. This increase has increased the demand for alternative energy sources. Therefore, the studies towards the development of new systems utilizing solar, wind, hydropower, and hydrogen as energy sources, as well as the components constituting these systems have been increased tramendeously [1].

The usage of solar radiation as an energy source in solar panels is one of the alternative energy types with a promising future for widespread use. Solar panels involves the electron transport mechanism within the system due to the exposure to sunlight, thereby, resulting in electrical current. One of the criteria effecting the efficient operation of the system is the use of high-performance transparent conductive oxide (TCO) layers [1].

TCO layers are photovoltaic materials with high electrical conductivity and optical transparency. Due to these properties, they are also used as front surface electrodes in solar panels.

Nowadays, indium tin oxide (ITO) films are widely used as TCO layers due to their high transparency in the visible region and low electrical resistance. However, zinc oxide (ZnO) films emerged as an alternative to ITO due to their non-toxic nature, low material cost, and high chemical stability properties [2].

TCO layers are typically prepared using thin film technologies such as spray pyrolysis, sol-gel, chemical or physical vapor deposition, laser deposition, and sputtering. It is possible to obtain fine fibers in nano size using the electrospinning methods [3,4].

Nanofibers carry fewer structural defects due to their small size, thereby possessing better mechanical and electrical properties.

Nanofibers can be produced through methods such as drawing, mold synthesis, self-assembly, and electrospinning. Among these production methods, nanometer-sized fibers can only be obtained through the electrospinning technique.

Electrospinning is a much simpler, cost-effective, and practical method compared to other techniques [5].

In this study, the aim was to enhance the electrical properties of ITO glass, which is a transparent conductive oxide layer used in solar panels for electron conduction, by coating it with Ag, ZnO, and TiO_2 nanoparticles doped via the electrospinning method.

CHAPTER II
LITERATURE REVIEW

2.1 SOLAR CELLS

Increasing energy demand and environmental concerns are driving interest in renewable energy sources today. In this context, solar energy stands out for its potential to provide sustainable and clean energy. Solar cells, which convert sunlight into electricity, are one of the most significant technological advancements in this field. Solar cells utilize the photovoltaic effect to directly convert sunlight into electrical energy.

Solar cells are typically made of thin layers of silicon or other semiconductor materials.

2.1.1 Main Components of Solar Cells

Solar cells directly convert sunlight into electrical energy using a phenomenon called the photovoltaic effect. A solar cell absorbs sunlight photons falling on its semiconductor material. These photons, by exciting the atoms within the semiconductor material, cause the movement of electrons. When the energy of sunlight is sufficient to separate the electrons (negative charge) and holes (positive charge) within the semiconductor material, an electron-hole pair is formed. This step occurs at energy levels within the band structure of the semiconductor. The generated electrons move in a specific direction within the material under the influence of electric fields present within the material. This directional movement creates an electrical current. Electrons are collected and an external circuit is established through electrical contacts placed on the top and bottom of the solar cell. These collected electrons carry a charge through the external circuit, generating an electric current. Electric current flows through an external circuit, moving a charge. This current can power an external load such as a lamp, device, or battery, or it can charge a battery.

P-N semiconductor junctions make up the majority of commercial solar cells because they provide the highest conversion efficiency [6]

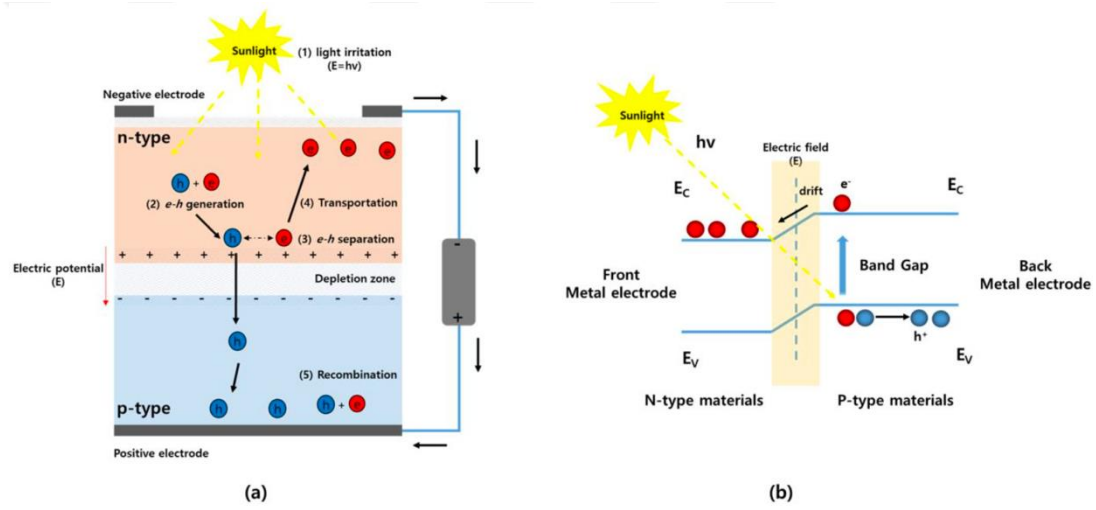

Figure 2.1: (**a**)P-N junction working principle, (**b**)Solar cell loss mechanism [6].

As seen in Figure 2.1 (a), a p-n junction is created by bringing together two different types of semiconductor materials: negative (n-type) and positive (p-type) materials. Industrial silicon is made from P- and N-type materials; this polarity is produced by doping the material with phosphorus (P) or boron (B). The depletion region forms around the junction contact when electrons and holes diffuse toward the opposite low charge concentration of each material.

Sunlight photons energy triggers the formation of electron-hole pairs in the depleted region of the junction. Basic PN-junction solar cells' loss methods are depicted in Figure 2.1(b) [6].

2.1.2 Types of Solar Cells

Due to the large number of types of solar cells, it is necessary to examine them in three main generations. These generations encompass different types of solar cells with varying technological and structural characteristics. Each generation is characterized by technological advancements and progress in research. As seen in Figure 2.2, there are three types of solar panel generations.

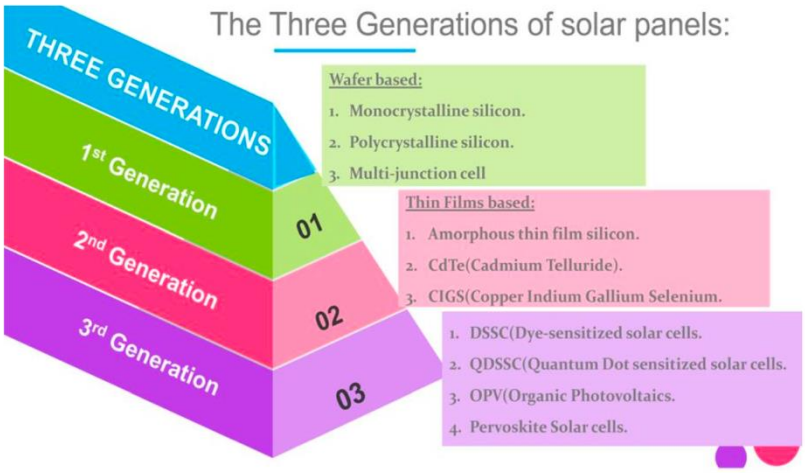

Figure 2.2: Generations of Solar Panels [6].

2.1.2.1 First Generation Solar Cells

The first generation of photovoltaic solar cells, which includes semiconductors like silicon and GaAs, is based on crystalline film production. Approximately 90% of the photovoltaic solar cell industry relies on silicon-based products, making silicon (Si) the most commonly used material for commercial purposes [7].

The most expensive method used in this technology is producing pure silicon crystals from crystalline Si. These solar cells are globally used and highly efficient [8].

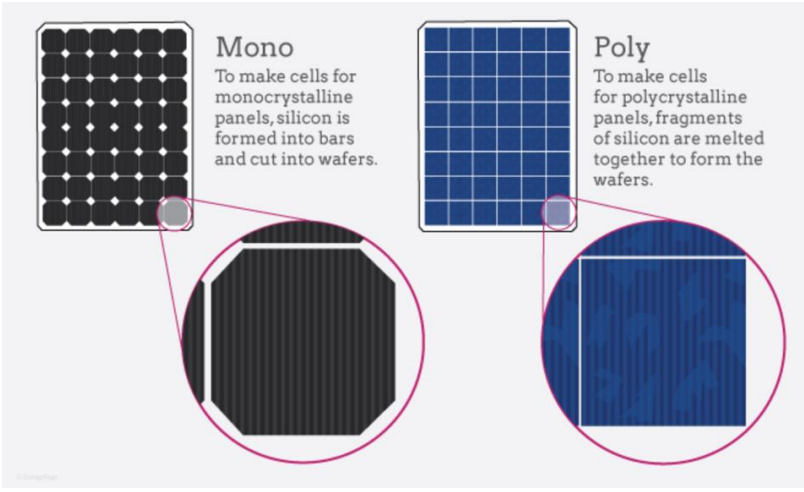

Figure 2.3: (**a**) Monocrystalline, (**b**) Polycrystalline solar cells [9].

Figure 2.3 (a) shows a monocrystalline solar cell, while Figure 2.1 (b) depicts a polycrystalline solar cell. The noticeable first difference between the two cells is that the corners of monocrystalline solar cells appear rounded. The reason for this is that

each cell is made from pure silicon. This ensures that the crystal structure is homogeneous and consists of a single crystal, which in turn provides higher efficiency.

Polycrystalline solar panels are also made of silicon, but instead of being formed from a single wafer, they are made from multiple silicon pieces. Silicon is melted and then cooled in fragments, which are later assembled before being cut into panels.

Around 80% of the market uses single crystalline solar cells. Monocrystalline solar panels typically have efficiency values ranging from 20% to 25%, while polycrystalline-based solar panels generally have efficiencies ranging from 13% to 16% [10]. According to Zhao et al. the efficiency of polycrystalline solar cells with a honeycomb structure is approximately 19.8%. Polycrystalline cells are less efficient than monocrystalline ones.

2.1.2.2 Second Generation Solar Cells

The main goal of second-generation photovoltaic solar cells is to reduce the cost, which was a primary issue with first-generation photovoltaic solar cells. Acquiring pure silicon is a complicated and expensive process. Reducing the cost of solar cells is feasible by depositing silicon thin films (1μm). Silicon usage in thin-film technology is significantly lower compared to wafer-based technology. R. Chittick pioneered the development of amorphous silicon deposited thin films [8,11]. Later, his colleagues published the first comprehensive and explanatory study on the plasma-enhanced chemical vapor deposition (PECVD) technique.

2.1.2.2.1 Amorphous Silicon Solar Cells

Amorphous silicon solar cells utilize non-crystalline silicon as the semiconductor material. These cells are known for their flexibility and ease of manufacturing, making them suitable for applications where traditional crystalline silicon cells may not be practical.

Amorphous silicon solar cells are the most developed thin-film solar cells. The structure typically consists of a p-i-n (or n-i-p) type of duality, where the p-layer and n-layer are usually used to create an intrinsic electric field (i-layer) and contain amorphous silicon [12]. The schematic of amorphous silicon (a-Si) cell structure is shown in Figure 2.4.

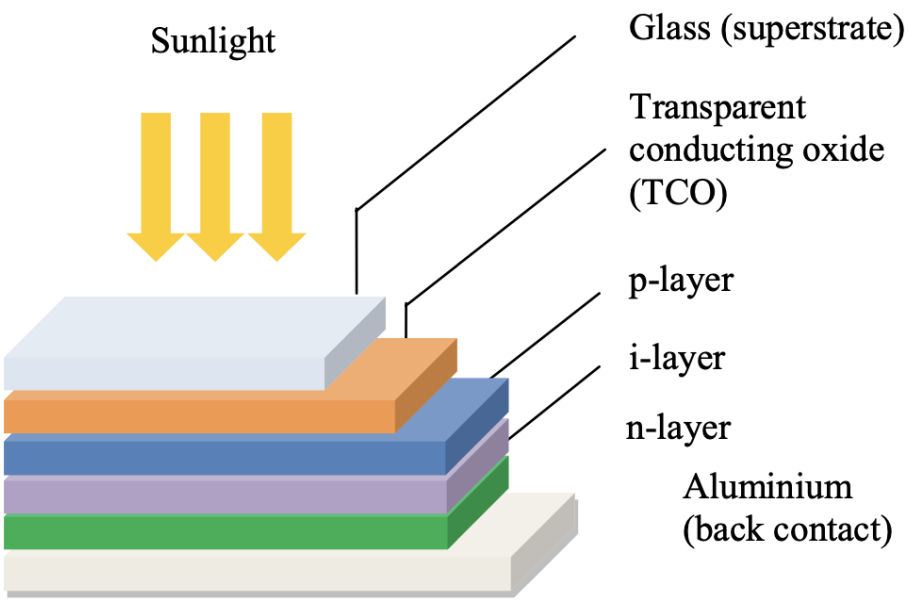

Figure 2.4: Schematic of amorphous silicon (a-Si) cell structure [13].

Three layers of amorphous silicon: the p-layer (doped p), the i-layer (intrinsic layer, naturally undoped internal layer), and the n-layer (doped n), are typically sequentially deposited on a glass substrate, which is commonly used as a superstrate, using the PECVD method with silane and hydrogen gas. The front contact utilizes transparent conductive oxide (TCO), while a reflective conductive layer (typically aluminum) serves as the back contact [13]. In a study aimed at improving the performance of amorphous silicon photovoltaic cells, stacking three p-i-n junctions instead of a single junction was investigated. This approach was reported to result in an efficiency of 13.4% [14].

2.1.2.2.2 Cadmium Telluride (CdTe)

Cadmium telluride solar cells rely on the p-n junction formed between two distinct materials. This design is referred to as a heterostructure. CdTe cells combines a p-doped Cadmium Telluride layer and an n-doped Cadmium Sulfide (CdS) layer as seen in Figure 2.5.

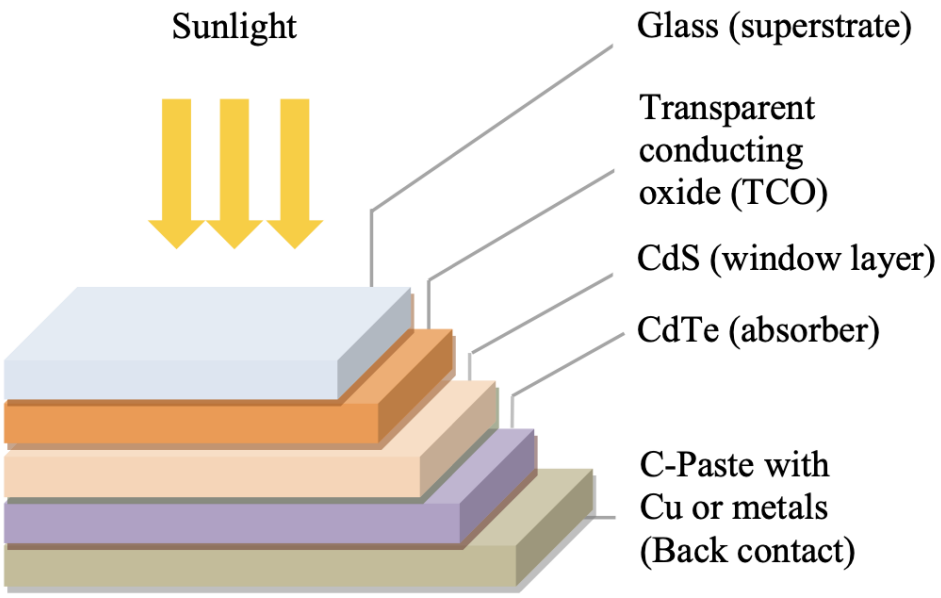

Figure 2.5: Schematic of CdTe cell structure [13].

The n-layer is a 'window layer' which is a transparent semiconductor with a wide bandgap (CdS). Photons passing through this layer are then absorbed by the CdTe layer, referred to as the 'absorber'. The solar cell is finalized by incorporating top and bottom contacts; a TCO is used as the front contact, while carbon pastes containing metal or copper are used as the back contact [13]. CdTe cells feature a straightforward design, are readily manufacturable, and achieve an efficiency of 19.6% [15].

Although CdTe competes with crystalline silicon in terms of cost/efficiency, a significant issue is the toxicity of cadmium. Therefore, special attention should be given to its recycling. An additional concern is that tellurium is an exceedingly rare metal on the world [16].

2.1.2.2.3 Copper Indium Gallium Selenium (CIGS)

CIGS cells are designed with a structure consisting of a CdS n-layer as a window layer, a thin CIGS p-layer used as the absorber, followed by a molybdenum (Mo) electrode layer over the substrate through a sputtering process used as the back contact and a TCO layer used as the front contact. The substrate is usually manufactured with polyimide or a metal foil as seen in Figure 2.6.

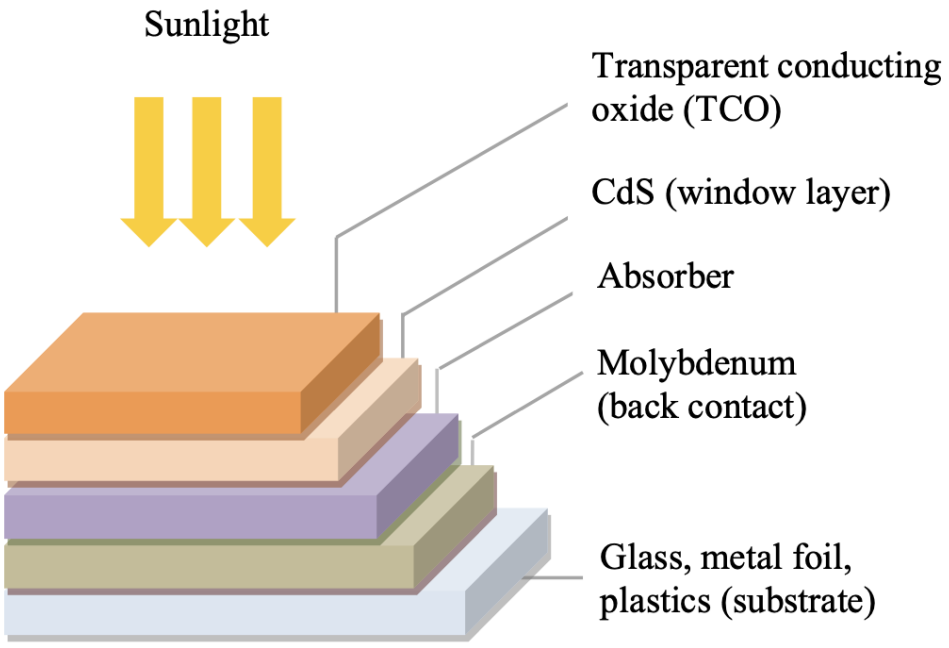

Figure 2.6: Schematic of CIGS cell structure [13].

Due to its composition of multiple elements, CIGS offers high flexibility to optimize certain properties, including bandgap and electron affinity. Therefore, the rare element indium can be partially substituted with sulfur in combination with gallium and selenium. These choices provide the opportunity to improve the performance of CIGS cells. Regarding production costs, current trends in CIGS research emphasize lower-cost deposition techniques such as non-vacuum methods and electroplating, offering alternatives to costly vacuum processes [13]. These efficiency and cost improvements have elevated CIGS as a leader among alternative cell materials.

2.1.2.3 Third Generation Solar Cells

Third-generation solar cells refer to advanced solar cell technologies and materials developed using more sophisticated approaches. These cells aim to achieve higher efficiency, lower cost, and broader application compared to first and second-generation solar cells. Examples of third-generation solar cells include perovskite, dye-sensitized, and quantum dot solar cells.

2.1.2.3.1 Dye Sensitized Solar Cells (DSSC)

DSSCs operate even under low light conditions like rainy or cloudy weather. This approach employs cost-effective materials, including natural dyes, and the

production process for DSSCs is simpler compared to high-cost silicon solar cells. Due to these advantages of DSSCs, extensive experiments are continuously conducted in this field. DSSCs offer a compelling alternative to costly crystalline Si technology [17]. DSSC cells can be manufactured using economical methods like inkjet printing, screen printing, or roll-to-roll printing [18]. Figure 2.7 illustrates the working principle of DSSCs.

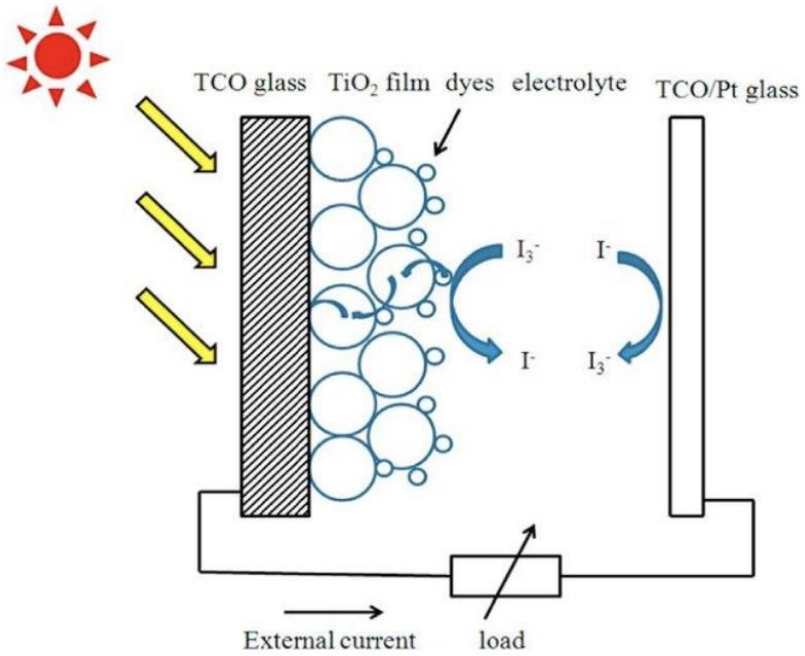

Figure 2.7: Schematic diagram of a DSSCs [18,19].

When sunlight hits the DSSC, a dye molecule absorbs the photons and becomes excited. This dye is typically made of a photosensitive organic dye or a metal complex. The excited dye molecule transfers its electron to the semiconductor material, which is typically titanium dioxide (TiO_2) coated onto a TCO glass. This process creates a negatively charged dye molecule and a positively charged semiconductor surface. The injected electron in the TiO_2 semiconductor material moves through the material towards the conductive substrate, while the positively charged dye molecule remains on the surface. The free electrons move through the conductive substrate towards the external circuit, creating an electric current. Meanwhile, the dye molecule, now positively charged, needs to be regenerated. This occurs through a redox reaction with a redox couple present in an electrolyte solution in contact with the TiO_2 layer. The redox couple accepts the electron from the dye, converting it back to its original state. This completes the cycle, allowing the dye molecule to absorb another photon and

repeat the process. The redox couple accepts the electron from the dye, converting it back to its original state. This completes the cycle, allowing the dye molecule to absorb another photon and repeat the process [20].

The use of synthetic dyes in DSSCs enhances efficiency and durability, but it can also result in increased costs and the use of toxic materials [17].

2.1.2.3.2 Quantum Dot Solar Cells (QDSC)

Quantum Dot Solar Cell, designed to absorb photons of sunlight for photovoltaic effect, utilizes quantum dots, which are tiny particles called quantum dots, on the nanometer scale. Quantum dots (QDs) are semiconductor particles that are a few nanometers in size, and their optical and electronic properties differ significantly from bulk materials [17]. The physics difference between bulk semiconductor and Quantum dots is illustrated in the Figure 2.8.

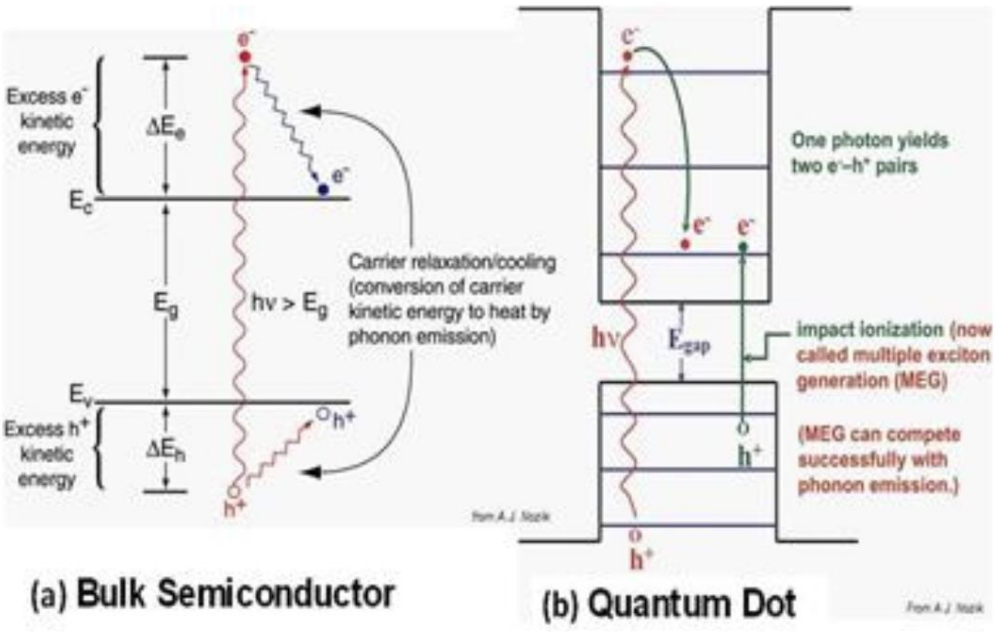

Figure 2.8: Difference between physics of Bulk material and QDs [17].

By altering the size, shape, and composition of the quantum dot, the emitted light frequency can be finely adjusted. Quantum dots of varying sizes and compositions emit light at distinct frequencies, which can be precisely controlled as required.

Quantum Dot Solar Cells are seen as an evolution from Dye-Sensitized Solar Cells. QDs like CdS [21], CdSe [22], PbS [23], and InAs [24] are utilized as

photosensitizers instead of organic dyes due to their versatile optical and electrical properties, including a tunable band gap dependent on the QD size.

Due to their tunable energy bandgap, QDSCs allow for much greater photon absorption, theoretically achieving up to 44% efficiency. Kim et al. demonstrated high-performance Zinc Oxide/Lead Sulfide heterojunction Quantum Dot Solar Cells, achieving a certified efficiency of 10.7%. This was accomplished by depositing durable self-assembled monolayers on the ZnO surface to adjust interface energy alignment [25].

2.1.2.3.3 Perovskite Solar Cells

The perovskite material consists of an ABX3 crystal structure. X can be a Br-, I-, or Cl- atom. Perovskite solar cells (PSCs) are more advantageous in production processes compared to silicon solar cells. Silicon solar cells require processing at high temperatures (e.g., around 1000°C) and specialized vacuum facilities to obtain pure silicon wafers. Therefore, the production of PSCs is easier and involves fewer steps [26]. In Figure 2.9, perovskite solar cells with p-i-n and n-i-p structures are shown.

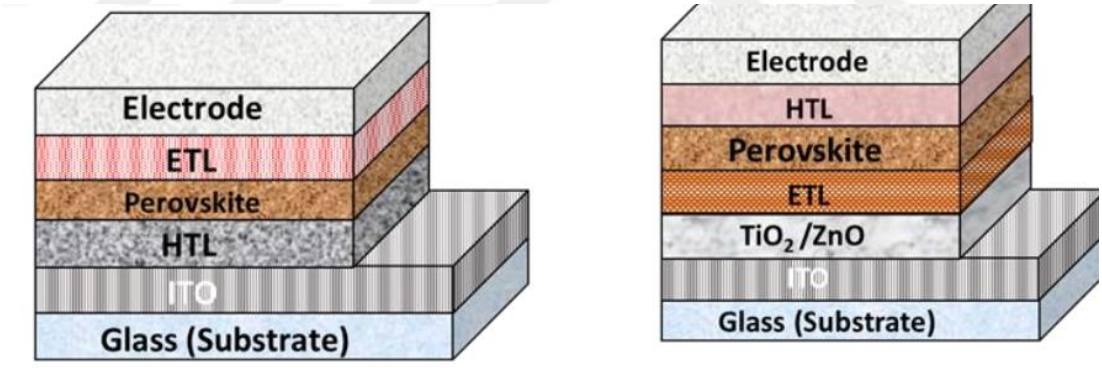

Figure 2.9: Layers of Perovskite Solar Cells [27].

A simple structured perovskite solar cell consists of 5 layers. These are the electrode, hole transport layer, perovskite layer, electron transport layer, and a transparent conductive oxide layer patterned on a glass substrate. Light incident on the perovskite layer generates electron-hole pairs, aligning these charges at desired energy levels to facilitate electron-hole flow. Holes move towards the electrode, while electrons move towards the TCO layer through the electron transport layer. This creates a flow of charge in a closed circuit, generating energy [28,29].

2.1.3 Variables That Affect The Efficiency of Solar Cells

2.1.3.1 Cell Temperature

A photovoltaic cell converts a small fraction, typically less than 20%, of incoming radiation into electrical energy, with the remainder being converted into heat. Module overheating often occurs due to excessive solar irradiation and high ambient temperatures [30,31].

Module temperature is a critical parameter that profoundly impacts the performance of a solar cell system as it directly affects efficiency and energy output. The primary effect of increasing cell temperature is the linear decrease in open-circuit voltage as cell temperature rises. The relationship between solar cells efficiency versus module temperature is shown in the Figure 2.10.

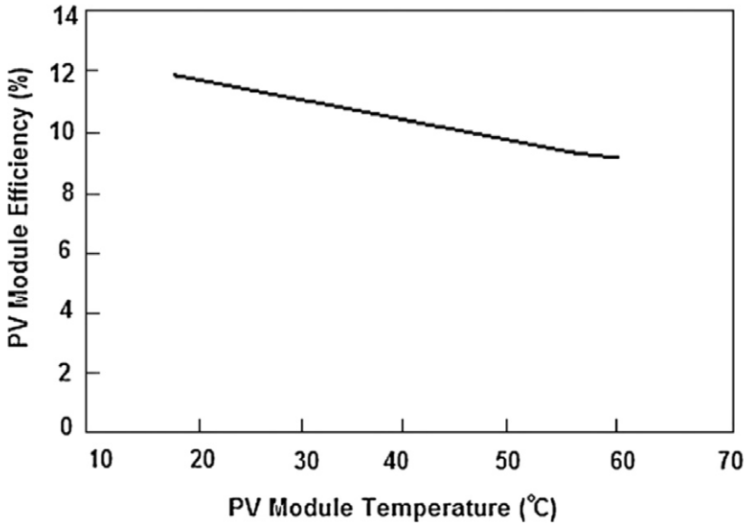

Figure 2.10: Solar cells efficiency versus module temperature [32].

The voltage of a cell decreases by around 2.2 mV for each 1°C rise in operating temperature, leading to a decrease in efficiency of crystalline solar cells by approximately 0.5% [32,33,34].

2.1.3.2 Solar Cell Material

The selection of photovoltaic (PV) materials can have substantial impacts on system design and performance. Among PV materials such as silicon, gallium arsenide (GaAs), copper indium diselenide (CuInSe2), cadmium telluride (CdTe), indium phosphide, and others, each exhibits varying cell efficiencies [35,36]. Single-crystalline cells typically have higher conversion efficiencies than multicrystalline

cells; that is, around 16-22% for single-crystalline cells and 14-18% for multicrystalline cells [37].

Single-crystalline silicon cells are one of the most efficient commercially available solar cell technologies, but they require larger amounts of raw materials compared to other technologies, which contributes to higher costs. In the thin-film technology category, efficiencies for other materials are approximately as follows: around 7-9% for amorphous silicon, 10-15% for CdTe, and 7-12% for CIGS cells [37].

Compared to crystalline silicon cells, thin-film cells exhibit higher thermal conductivity due to their thinner structure, enabling more efficient dissipation of heat from the solar module. A recent advancement includes dye-sensitized solar cells, which have achieved peak laboratory efficiencies of 12.3% on glass substrate and 8.6% on flexible stainless steel substrate [38].

2.1.3.3 Band-gap energy

When sunlight photons strike a solar panel's surface, only those possessing a requisite energy level can liberate electrons from atomic bonds, producing an electric current. What liberates these electrons is the energy needed to transition an outer shell electron from the valence band to the conduction band, termed the bandgap energy. The bandgap energy varies among different materials and even among different atomic structures of the same material. Crystalline silicon, for example, has a bandgap energy of 1.1 electron-volts (eV). The bandgap energies for other solar cell materials range from 1 to 3.3 eV [39,40].

2.1.3.4 Solar Panel Efficiency

The energy conversion efficiency of a solar panel is defined as the ratio of the power converted from absorbed light into electrical energy to the rated power of the panel. This efficiency depends on various factors such as the surface area of the panel and the properties of the materials used. Additionally, it is important for the TCO material used in the solar cell to have a high conductivity coefficient to ensure that the generated electrical energy can be transmitted with minimal loss [32].

2.2 TCO LAYERS

In general, TCOs are degenerate n-type semiconductors intrinsically doped with local donors such as oxygen vacancies, and additionally doped with extrinsic donor

impurities. There is a natural limitation in the conductivity of metal oxide that can be achieved by increasing the carrier concentration, because the Coulomb interaction between free electrons and ionized donor centers generated from them provides a scattering source specific to the doped material [41,42].

2.2.1 Applications

Due to their excellent optical transparency and conductivity properties, TCO materials are utilized in a wide range of applications. TCO thin films are commonly used in flat panel displays, laptop screens, gas sensors [43,44].

Transparent conductive oxide layers are also found applications in the rear defrosting windows of automobiles, as well as in oven glass with touch applications and solar cells. Furthermore, transparent conductive oxide layers can be used on the back surfaces of solar panels to increase short-circuit current [45,46]. They are the most crucial components of solar cells due to their high electrical conductivity and high optical transparency. Their ability to transmit light, while also conducting electrical current is their most significant factor. TCO layers are used in solar cells as either front surface electrodes or as part of the rear surface reflector.

In applications, where transparent conductive oxide layers are used as front surface electrodes, they need to have properties such as high transparency in the visible region and high electrical conductivity. While these are necessary characteristics for good transparent oxide layers, they are not sufficient on their own. In addition to this, transparent conductive oxide layers need to have excellent light-capturing capabilities [47]. In addition, transparent conductive oxide layers used in solar cells are aimed to achieve the lowest sheet resistance values (<10^-3 Ω.cm) and the highest optical transparency (%80 <) in the desired morphological and crystal structure.

2.2.2 Types and Properties

TCO layers can be produced from a variety of materials, including semiconducting oxides such as tin, indium, zinc, and cadmium, as well as a wide range of other materials such as gold, silver, and titanium.

Most TCO materials exhibit n-type conductivity, where the majority of free carriers are electrons (e.g., In2O3, SnO2, and ZnO), but p-type conductivity is also available (e.g., CuAlO2, SrCu2O2, and NiO). Both types create donor states by introducing defects in the crystal structure, near the conduction band for n-type and in

the valence band for p-type. These states should be shallow to preserve transparency. These materials find a wide range of applications in the solar cell industry [48].

The efficient performance of transparent conductive oxide layers is contingent upon their ability to possess high electrical conductivity and low optical absorption in the visible region simultaneously. Criteria used in the selection of transparent conductive oxide layers include[49]:

- High transparency in the solar spectrum range,
- High conductivity,
- High carrier mobility,
- Appropriate refractive index,
- Capability for enlargement and roughening for proper light scattering,
- High chemical stability,
- Non-toxicity,
- Low cost.

Indium Tin Oxide films (ITO) are widely used as transparent conductive oxide layers today due to their high transparency in the visible region and low electrical resistance [1]. ITO is a type of thin film coating formed by the oxidation of indium and tin.

Indium tin oxide ($In_{2-x}Sn_xO_{3-x}$) is formed when tin (Sn) is doped into indium oxide (In_2O_3). As a result, tin forms an intermediate bond with oxygen, resulting in the formation of SnO or SnO_2 . Additionally, in ITO films, tin (Sn) and oxygen (O) vacancies contribute to high conductivity. The direct optical band gaps of ITO films are generally larger than 3.75 eV, and different values ranging from 3.4 to 4.06 eV have been reported in the literature [50] Their high optical transparencies result from their semiconductor properties with wide band gaps.

These films can be applied to substrates such as glass or plastic and have wide-ranging applications due to their high conductivity and optical transparency. They are commonly used in electronic devices such as smartphone screens, touch panels, solar cells, and LCD displays [51].

2.2.3 Production Tecniques of TCO layers in Solar cells

Fluorine-doped tin dioxide (SnO2:F) is widely used as TCO in architectural applications, as well as in thin films of A-Si and cadmium telluride (CdTe), and in energy-efficient windows.

Indium tin oxide (ITO) doped with tin is widely used in PV modules, including flat panel displays (FPDs), high-resolution televisions, and certain types of solar cells based on a-Si or (CIGS). Currently, crystalline and polycrystalline silicon solar cells, which dominate the TCO market for solar cells, represent 93% of the current market [52]. The types of TCO used by which solar panels are shown in Figure 2.11.

Cell Type	TCO in Current Use	TCO Needs	Materials Goals
Heterojunction with intrinsic thin layer (HIT) cell	Indium tin oxide (ITO)	Smooth, good interfacial properties, very good conductivity, low-temperature deposition, light trapping	Indium zinc oxide (IZO), indium-free materials, ZnO
Copper indium gallium selenide (CIGS)	Intrinsic-ZnO/Al:ZnO	Interfacial stability to CdS, low-temperature deposition, resistance to diffusion and shorting, need to make/improve the junction	Single-layer TCO to replace two layers and CdS layer
CdTe	(SnO_2) Zn_2SnO_4/Cd_2SnO_4	Stable interface to CdS/CdTe at temperature, diffusion barrier	Doping of ZnSnOx materials, single-layer TCO
Nano-hybrid polymer cell	ZnO, SnO_2, TiO_2	Nanostructure with right length scale, work-function matching, interface with organic, correct doping level for carrier transport	Self-organized structures core–shell structures, new nonconventional TCOs
Grätzel cell	TiO_2	Nanostructure with high electron mobility	Improved TiO_2 morphology and possible use of doped materials, new non-TiO_2 materials
Amorphous Si	SnO_2, ITO, and ZnO; many cells employ two TCOs	Temperature stability, chemical stability, and appropriate texture for both TCO layers	Higher conductivity, texture, and ohmic contact for both TCO layers

Figure 2.11: TCOs Employed in Solar Cells [53].

2.3 NANOFIBERS

Nanofibers are defined as fibers with diameters of one micron and below. They are produced in nanoscale dimensions from polymer solutions using various methods.

The shapes of nanofibers typically resemble thin threads [54]. Nanofibers are lightweight, highly porous, and have a large surface area, making them advanced materials with high functionality and mechanical strength. The advantages provided by nanofibers can be listed as follows: increased surface area per unit mass, high performance in filtration, significant improvement in fabric performance properties such as waterproofing, stain resistance, and wrinkle resistance.

Nanofibers find applications in various fields such as filtration, tissue engineering, sensor fabrication, production of protective masks and clothing, drug delivery, catalyst support, wound dressings, polymeric batteries, and composite reinforcement [55]. Dharani et al. reported that TiO2 nanofibers' good electrical and morphological properties, along with the high extinction coefficient of CH3NH3PbI3 perovskite, have been combined to achieve a solar cell with a power conversion efficiency of 9.8% [56].

2.3.1 Nanofiber Production Techniques

Nanofibers are produced using methods such as drawing, template synthesis, phase separation process, self-assembly, and electrospinning. The electrospinning technique is the most widely known and easily applicable method for the production of this material. With this method, ultra-fine nanofibers (100-1000 nm) are produced from various liquid polymers (such as PVA)[57].

2.3.1.1 Drawing Method

In this method, a micropipette with a few micrometers in radius is used. The micropipette is immersed into the polymer droplet with the help of a micromanipulator and then pulled away from the droplet at a speed of approximately 10^-4 m/s. This way, fibers are collected on a surface. The pulling of nanofibers is repeated several times on each droplet [58]. The steps of the drawing process are shown in the Figure 2.12. The disadvantages of this method is the formation of discontinuous fibers and fiber with diameters being larger than 100 nm, which render its practical usage.

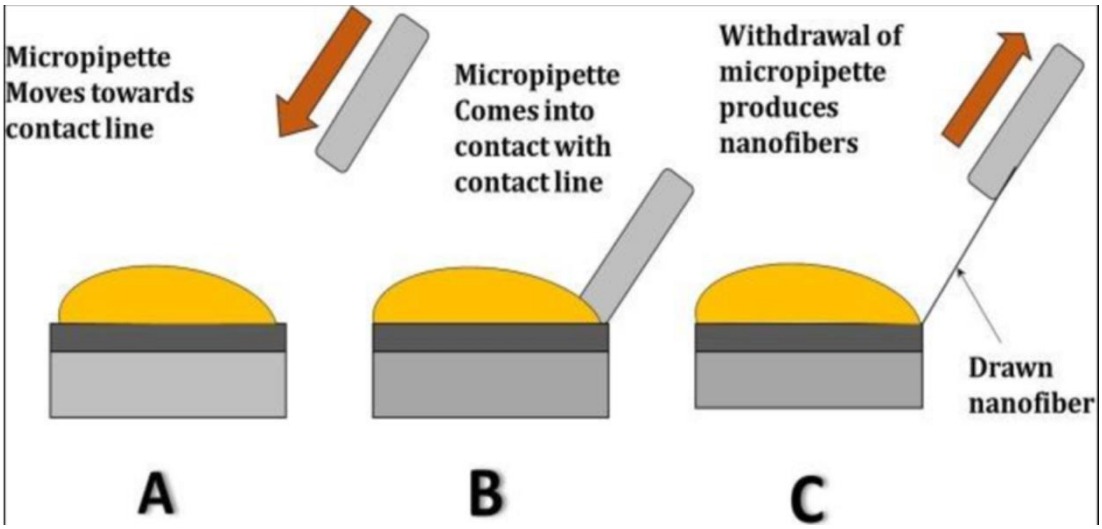

Figure 2.12: Drawing method steps [59].

The disadvantages of this method include fiber diameters being larger than 100 nm and its discontinuous nature, rendering it practically unusable.

2.3.1.2 Template Synthesis

This method requires the use of a mold or template to obtain the desired material or structure. Ferg et al. [60] used a metal oxide membrane across the dimensions of the pores to control the state of nanofibers created.

The membranes are 5–50 mm thick and have cylindrical pores. Each pore can be seen as a vessel where the desired nanostructure is synthesized.

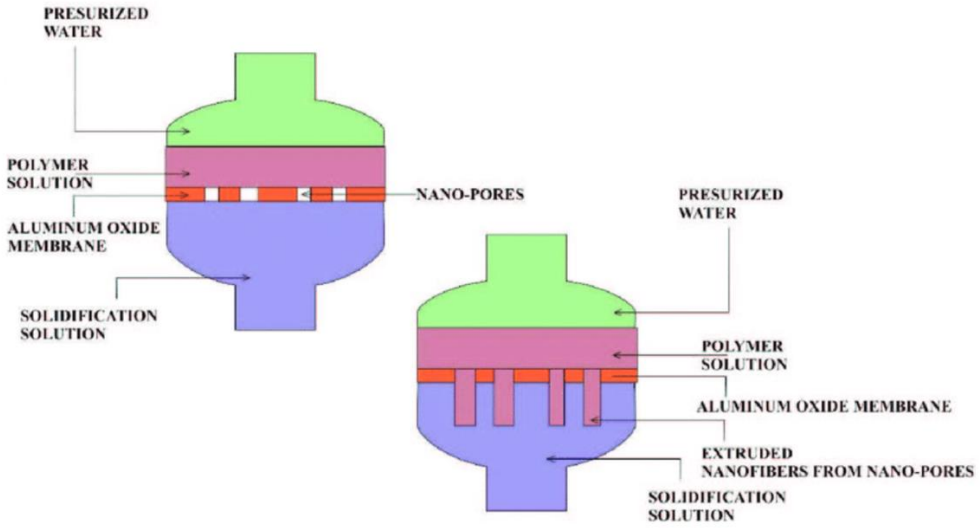

Figure 2.13: A typical process of obtaining nanofibers by template synthesis [61].

The passage of the polymer solution through the membrane is achieved by water pressure (Figure 2.13). As soon as the polymer encounters the solidifying liquid, fibers are formed. The diameters of the fibers range from a few nanometers to 100 nanometers [62].

2.3.1.3 Phase Separation Process

The basis of the method relies on the thermodynamic separation of a homogeneous polymer solution into two distinct phases: a polymer-rich phase and a polymer-poor phase [63].

In phase separation, a polymer is initially mixed with a solvent before gelation occurs. One of the phases (i.e., the solvent) is then removed from the gel-like phase (Figure 2.14). The steps for producing are as follows:

- Polymer dissolution: The polymer is dissolved in a suitable solvent.

- Gelation: Suitable chemical substances are added to induce gelation of the polymer, then the mixture is placed in a Teflon bottle and refrigerated to allow gelation to occur.

- Solvent removal: To remove the solvent, the Teflon bottle is placed in pure water, and left for 2 days. During these two days, the pure water is changed three times a day.

- Freezing: The gel in water is removed and filtered through a paper sieve, then left to freeze at -18°C for 2 hours.

- Freeze-drying: The frozen gel is transferred to freeze-drying chambers and left at -55°C for 1 week [58]

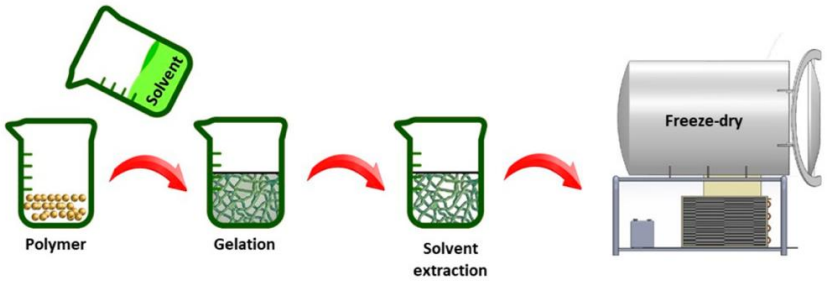

Figure 2.14: Phase Separation production steps [64].

2.3.1.4 Self-Assembly

Nanofiber production is achieved by assembling blocks with small molecules. Initially, small molecules are arranged in a concentric manner to form bonds between them. Subsequently, the substantial merging of these molecules results in the formation of nanofibers as shown in Figure 2.15. The smallest unit formed determines the shape of the macro-molecular fibers [58,65].

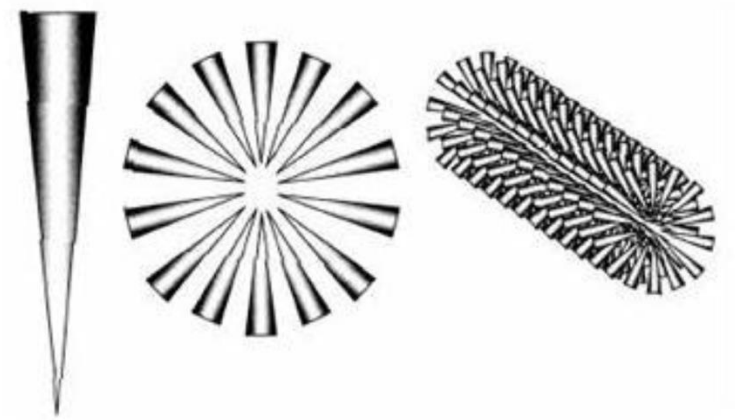

Figure 2.15: Production of nanofibers by the self-collection method [58].

2.3.2 Electrospinning

Electrospinning is a fiber production technique that employs a top-down engineering approach to draw ultra-fine fibers from polymer melts using electrical forces. The process, while not a new technology, originated in the 1600s when William Gilbert, conducting research on magnetism, serendipitously observed the effect of electromagnetism on liquids. In his work, Gilbert noted the electrical attraction of a water droplet being drawn towards a dry surface at a certain distance in a conical shape. This event marks the inception of the history of electrospinning [66].

The electrospinning technique offers a different approach for producing fibers with diameters ranging from a few nanometers to several micrometers by forming a jet from an electrically charged polymer solution or melt [67]. It is a voltage-driven technology that uses an electro-hydrodynamic process, in which a high voltage is applied to the polymer solution and then a liquid droplet is electrified to generate a jet, followed by elongation and stretching to produce fibers [68]. A basic electrospinning setup includes an injection pump to deliver the spinning solution, a needle attached to

a syringe, a voltage power supply, and a collector positioned at an optimal distance (Figure 2.16) [69].

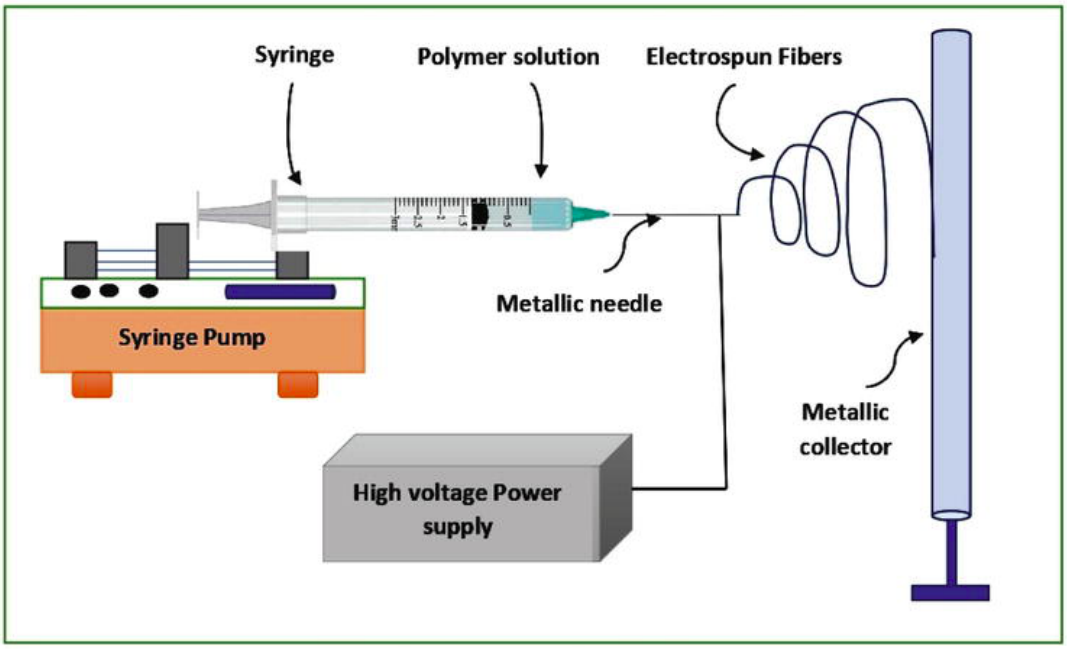

Figure 2.16: Basic setup of electrospinning [70].

The electrospinning involves applying high voltage to the needle at the tip of the syringe, while the syringe pump pushes the polymer solution inside the syringe to form droplets at the needle tip.

In principle, four successive processes are fundamental in generating the fiber jet from the polymer droplet. Positive charges gather around the droplet because of the high voltage applied to the polymer solution at the needle tip. With increased voltage, the surface tension of the polymer at the needle tip cannot withstand the repulsive force of the charges, causing the droplet to form into a conical shape known as the Taylor cone, as depicted in Figure 2.17 [69].

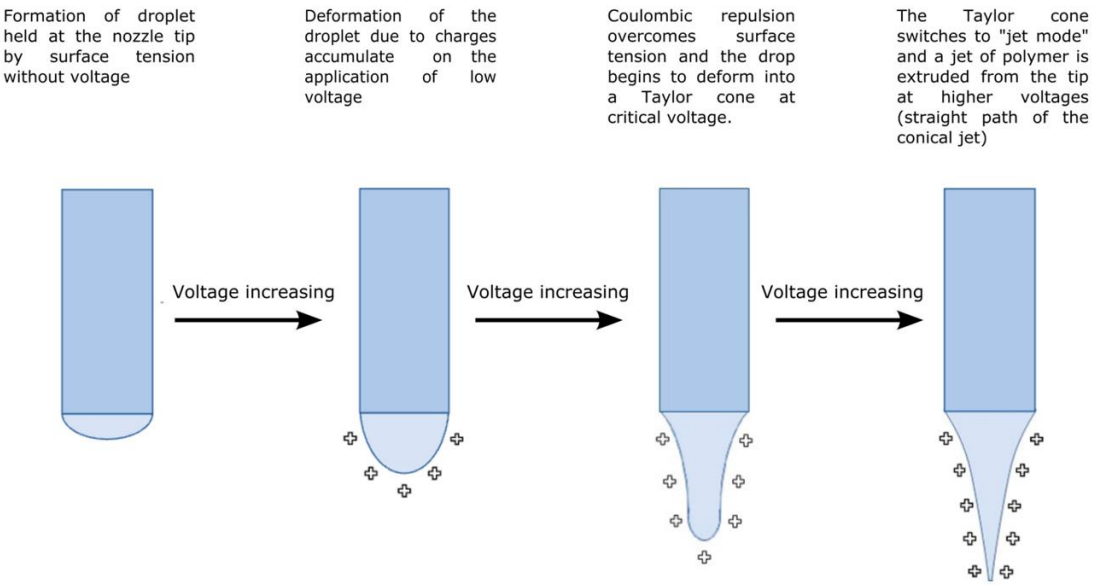

Figure 2.17: Modes of deformation exhibited by polymer droplets or jets during the electrospinning process [71]

After the formation of the Taylor cone, the droplet retains fewer positive charges compared to the polymer jet. A continuous stream of fibers is ejected from the apex of the Taylor cone towards the collector under critical voltage. As the jet approaches the collector, the concentration of surface charges increases [72-73]. After complete evaporation of the solvent during the ejection of the jet, solid fibers accumulate on the collector, resulting in a fibrous, textureless surface [5].

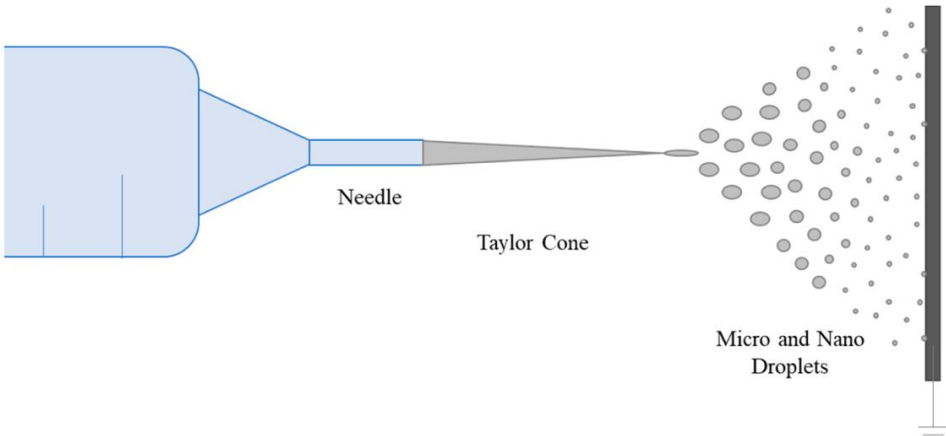

Figure 2.18: Schematic representation of the electrospraying process [71].

2.3.2.1 Electrospinning Parameters Used in Production of Nanofibers

The parameters affecting the electrospinning process are the applied voltage, the diameter of the metal needle tip, the distance between the needle tip and the collector, and the polymer solution used.

2.3.2.1.1 Voltage

While it is understood that the electric field strength escalates with higher applied voltage, achieving the necessary cone for fiber formation demands a critical voltage, even when the operating distance is minimum due to the high electric field force. This imbalance leads to a broad size distribution in the resulting fibers when high voltage is applied [74]. It is known that the applied electrical voltage significantly influences the morphology of the fiber. To create continuous fibers, it is necessary to balance the surface tension of the solution with the electrostatic force. Once the applied voltage surpasses the critical threshold, liquid jets will be expelled from the tip of the cone. If the viscosity of the solution is extremely low, the jets responsible for bead formation will not be stable. High voltages can generate more charge on the surface of the solution or droplet at the tip of the needle (higher Coulomb forces) and create a stronger electric field (larger electrostatic forces), both of which act effectively to fully stretch the jets, leading to the formation of homogeneous and uniform fibers [75,76].

2.3.2.1.2 Feed Rate

A low feeding rate causes a vacuum to form inside the needle; however, higher feeding rates lead to polymer buildup at the edge of the needle tip and disrupt the formation of the Taylor cone. A precise feeding rate value is essential to achieve and sustain a stable Taylor cone at each applied voltage [77,78]. It has been noted that the feed rate of the polymer solution significantly influences the morphology of the polymer fibers. There is also an optimum value for the feeding rate. If the feeding rate is higher than the optimum value, it leads to the production of fibers with beads, which is an undesirable outcome.

2.3.2.1.3 Tip-to-Collector Distance (TCD)

The TCD mainly impacts the solvent evaporation in the solution and the stretching of a PVA macromolecular chain, while also influencing the strength of the electric field. As TCD decreases, the strength of the electric field increases. The

polymer jets undergo stretching due to electrostatic forces as they traverse through the electric field. Throughout this process, the solvent evaporates, allowing the polymer jets to maintain their flexibility.

If a decrease in fiber diameter is observed, gradually increasing the working distance achieves an optimum point to achieve uniformity; beyond this point, increasing the distance further can lead to decreased uniformity of the fibers, and in some cases, cracks may appear in the PVA fibers. However, as demonstrated in Phachamud's experiment, varying the TCD within a narrow range of 10 to 15 cm did not inhibit the formation of thin fibers or defects [74].

The SEM images chosen in Figure 2.19 illustrate the morphological characteristics of fibers derived from a sonicated 10% w/v PVA solution collected at different distances, ranging from 5 to 20 cm [79].

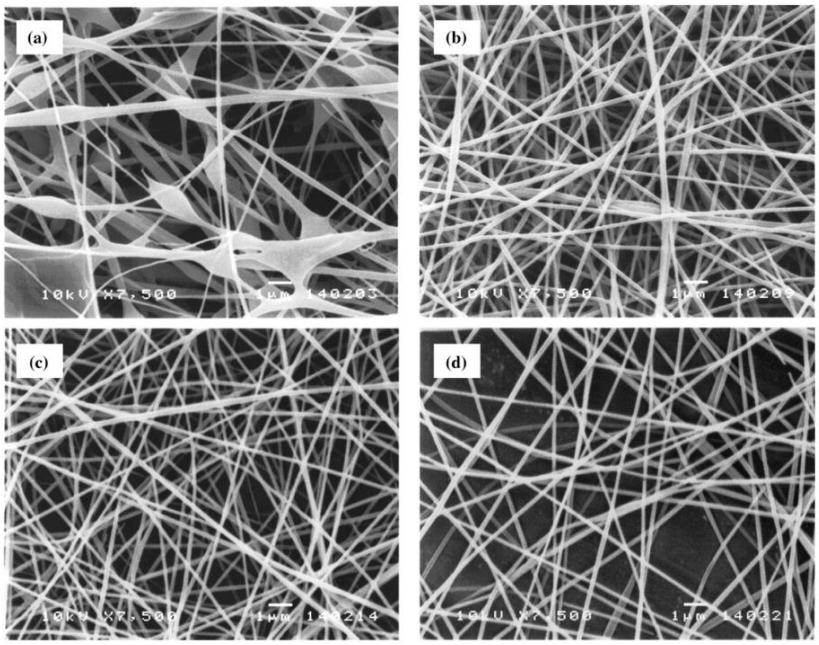

Figure 2.19: SEM images distances of (**a**) 5, (**b**) 10, (**c**) 15 or (**d**) 20 cm [79].

Clearly, at a collection distance of 5 cm, a mixture of straight and beaded fibers is obtained, with some adjacent fibers seen to merge at their contact points. This suggests that the jet did not completely dry before landing on the collector. As the distance between the needle tip and the collector increases, the electric field's strength diminishes, leading to a reduction in electrostatic and Coulomb repulsion forces. These adjustments result in instability in the emission of the solution jet, leading to a longer

flight path. This extended flight path facilitates solvent evaporation and the stretching of polymer jets to produce fibers of smaller diameter. On the contrary, a decrease in TCD generally leads to incomplete solvent evaporation, resulting partly in the dissolution of swollen fibers, forming larger diameter or non-beaded fibers. Thus, increasing the distance between the needle tip and the collector is essential to achieve uniform and homogeneous fibers or micro-particles.

2.3.2.1.4 Types of Polymer Solutions

A variety of synthetic and natural polymers are employed in the electrospinning technique. These polymers can form fibers in the submicron range and find applications in various fields. Electrospun nanofibers can consist of natural polymers, synthetic polymers, or a blend of both, and may also incorporate proteins, polysaccharides, and nucleic acids [80]. Natural polymers possess the capability to bind with cells, making them particularly suitable for use in electrospinning processes, especially in biomedical applications. Examples of natural polymers include chitosan [81,82] ,hyaluronic acid [83], gelatin [84], collagen [85,86], and silk protein [87,88]. Synthetic polymers typically offer several advantages over natural polymers, such as the ability to control degradation rates and achieve specific mechanical properties [89]. Numerous synthetic polymers are utilized in electrospinning, including poly(ε-caprolactone) (PCL), polylactic acid (PLA), polyethylene oxide (PEO), and polyvinyl alcohol (PVA) [90,91].

Polyvinyl alcohol (PVA) is a water-soluble polymer with numerous hydroxyl groups attached to the side chains. It has been extensively studied due to its high hydrophilicity, processability, biocompatibility, good physical and mechanical properties, complete biodegradability, excellent chemical resistance, and its ability to form films effectively. Due to its antibacterial properties, it has led to its widespread industrial use in applications such as drug delivery and medical dressing membranes. [3]. Recently, with the increasing popularity of electrospinning applications, the popularity of PVA among polymer solutions has also risen.

PVA is available in various degrees of hydrolysis (DH). This variation has also influenced the sizes of the fibers formed as a result of electrospinning. In fact, it has been possible to produce very fine fibers with a diameter of approximately 190 nm from PVA with a hydrolysis degree of 89%.[57].

As a result, electrospinning is widely preferred in applications because it allows for the control of fiber sizes by altering the properties of PVA independently of electrospinning parameters.

Some experiments were conducted to determine the optimum solvent content for dissolving PVA polymer and to get a solution which can be electrospinned easily. In these experiments, Dimethylformamide (DMF), acetone, chloroform, and distilled water were used as solvents. It was observed that DMF, acetone, and chloroform did not dissolve PVA uniformly, while distilled water dissolved PVA homogeneous [66].

Although such solvents are used in the literature, in this study, the PVA solution was prepared using distilled water as the solvent. This has allowed for both lower costs and more environmentally friendly production by reducing the use of chemicals.

2.4 NANOPARTICLE ADDITION TO NANOFIBERS DURING PRODUCTION BY ELECTROSPINNING

Various nanoparticles added to PVA, such as silver, are used to enhance the antibacterial property of PVA solution, while silver, titanium dioxide and zinc oxide nanoparticles are added to improve their electrical properties.

2.4.1 Types of Nanoparticles

2.4.1.1 Silver Nanoparticles

Silver is a precious element that has been used in a wide range of fields such as jewelry making, coinage, and explosive production for thousands of years. In the 17th and 18th centuries, silver nitrate was used in the treatment of acne, and epilepsy. The antibacterial properties of silver and silver salts were identified after the discovery of bacteria, leading to various applications aimed at preventing infections. Although the discovery of antibiotics has led to a decrease in the use of silver compounds and ions, research on the antibacterial properties of silver has gained popularity with the development of antimicrobial resistance [92].

Silver nanoparticles are clusters of metallic silver atoms at the nanoscale, exhibiting not only antibacterial properties but also high thermal and electrical conductivity [93].

For these reasons, silver nanoparticles were added to the PVA solution, and thin film coatings were applied using electrospinning to investigate the electrical properties of silver nanoparticles.

2.4.1.2 Zinc Oxide (ZnO)

Zinc oxide (ZnO) is an inexpensive and non-toxic material. Additionally, it meets the necessary properties for electro-optic devices. Zinc oxide holds an important place in semiconductor studies. ZnO, ease of sintering and controllable electrical resistance, coupled with its excellent electrical, optical, and chemical properties. Therefore, it finds applications in various fields such as semiconductors, optics, piezoelectric devices, transparent electrodes, and solar cells. It also exhibits antibacterial properties, like silver [94].

Films prepared with ZnO compound are preferred among metal oxide semiconductors due to their optical transparency and high electrical conductivity, despite reflections in the visible region [95].

The reason for using zinc oxide as an additive in the PVA solution is to observe the change in electrical properties by fabricating a thin film coating on the surface of TCO/ITO glass, which is conductive material, using the electrospinning method

2.4.1.3 Titanium dioxide (TiO_2)

Titanium dioxide (TiO_2) is an ideal photocatalyst due to its stability in terms of chemical and optical properties. There are several methods for producing TiO_2 in composite form, including freeze-drying, thermal evaporation, and physical and chemical vapor deposition. However, these methods are considered slow and costly due to their multiple steps [96].

Recently, there has been a growing interest in the use of electrospun TiO_2 for various applications, as the nanofibers have greatly enhanced photocatalytic performance owing to their small size. This results in rapid charge transfer dynamics and electron-hole recombination on the large specific surface area of TiO_2 nanofibers. Nanometer-sized titanium dioxides are utilized in applications such as fiber optic cables, photocatalysis, and solar panels [96].

For the production of composite fibers containing TiO_2, the electrospinning method is more popular compared to others.

CHAPTER III
EXPERIMENTAL STUDIES

In this part of the thesis, the materials used in electrospinning, and the solution preparation and electrospinning procedures are explained with the characterization techniques employed in the study.

3.1 RAW MATERIAL

In this study, nano particle doped Polyvinly Alcohol (PVA) nanofibers are coated on Indium Tin Oxide (ITO) glass substrate via electrospinning technique. The properties of nano powders, namely, Ag, ZnO and TiO2 are presented in Table 3.1 with the PVA particles from which doped electrospinning solution was obtained. PVA particles formed in granule form.

Table 3.1: Properties of raw materials used during electrospinning

Materials	**Mean Particle Size (nm)**	**Purity (%)**	**Supplier**
Ag powder	100	99.99	Sigma-Aldrich/Germany
ZnO powder	100	99.99	Sigma-Aldrich/Germany
TiO_2 powder	100	99.99	Sigma-Aldrich/Germany
PVA paticles	-	99.00+	Sigma-Aldrich/Germany

ITO glass is a material that typically combines electrical conductivity and optical transparency. The thickness and electrical properties of the ITO glass used in this experiment are provided in Table 3.2.

Table 3.2: Properties of the TCO/ITO glass

Parameters	**Values**
Resistance (Ω)	34.0
Thickness(mm)	2.240

3.2 SOLUTION PREPARATION FOR COATING

Firstly, preperation of PVA solution, nanoparticles are added to PVA in different contents and ITO glass were coated with doped fibers using electrospinning technique.

3.2.2 Preperation of PVA Solution

PVA solutions were prepared by adding 1 gr of PVA powder to 10 ml of distilled water to achieve obtain a PVA solution by 10 %wt. The solution was prepared in two steps, which were presented in Table 3.3

Table 3.3: The preparation values for PVA solutions.

Parameters	**1. Step**	**2. Step**
Temperature (°C)	85	Room temperature (22)
Time(hour)	2	24
Stirring speed (rpm)	600	300

Initially, the PVA solution containing beakers were covered with aluminum foil and heated at 85 degrees for 2 hours while being stirred at 600 rpm using a hot stage magnetic stirrir. Afterwards, the solution was stirred at room temperature at 300 rpm for 24 hours. The setup for preparing the PVA solution is shown in Figure 3.1.

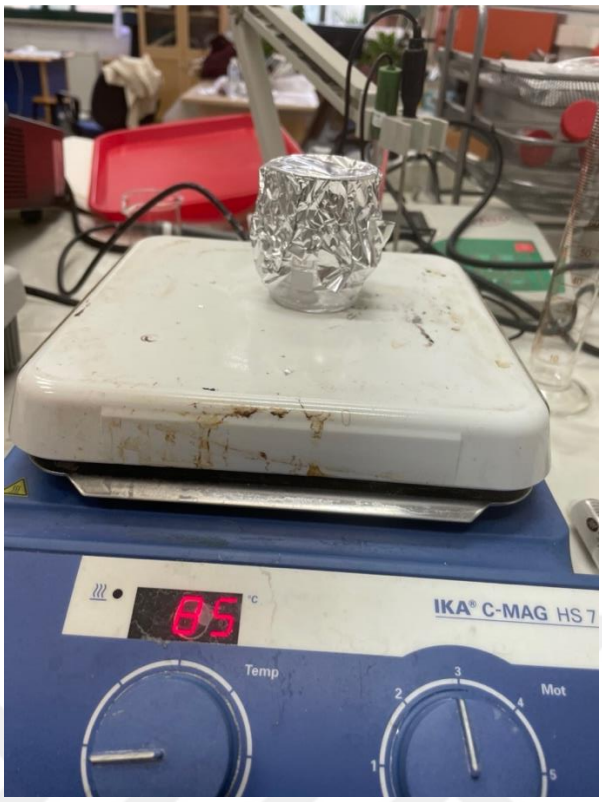

Figure 3.1: The mixing and heating of PVA powders with distilled water.

3.2.3 Nanparticle Doped Solution Preparation

After preparing the PVA solutions, Ag, ZnO, and TiO_2 nanopowders were added to the polymer solution at different quantities to form PVA solutions doped with nano particles. Prepared nanoparticle doped solutions are presented in Table 3.4. The nanoparticles concentration was changed between 0.03 and 0.2 gr in 10 gr of solution. Since the addition of nanoparticle changes the solution color as seen in Figure 3.2, the maximum content of the nanoparticles was kept at 5 wt. %, beyond which transparency of the solution was lost. However, fiber production by addition of 10 and 20 wt.% nanoparticles was also tried.

Figure 3.2: PVA solution with %Ag.

Table 3.4: Amounts of nanoparticles added to PVA solution (10 wt.%)

Type of Nanoparticles	**Amount of Nanoparticles**			
	3 wt.%	5 wt.%	10 wt.%	20 wt.%
Ag	0.03 gr	0.05 gr	0.1 gr	0.2 gr
ZnO	0.03 gr	0.05 gr	0.1 gr	0.2 gr
TiO_2	0.03 gr	0.05 gr	0.1 gr	0.2 gr

As can be seen in Table 3.4 twelve diffrent nanoparticle added solutions were prepared. The ensure the homogenous distribution of nanoparticles in the solution, all of the solutions were stirred for 2 h at 650 rpm in a magnetic stirrer at room temperature.

3.3 THIN FILM COATING BY ELECTROSPINNING

The electrospinning application was carried out using the Electrospinning device (OptoSense) in the Materials Science Laboratory at Yildiz Technical University, Davutpasa Campus/Istanbul.

Figure 3.3: Electrospinning device used in electrospinning studies.

The experimental set-up is shown in Figure 3.4 **(a)**. The target ITO material, which was to be coated with nanofibers, was attached to the aluminum foil fixed on perpendicular plate (Figure 3.4 **(b)**). The role of the aluminum foil was to facilitate the easier progression of the electric current supplied to the syringe tip through the aluminum foil. Carbon tape was preferred for its conductivity to achieve a more homogeneous coating on the glass surface. The ITO glass utilized in coating process was conductive in one side and it was acting as non -conductive at other surface. The coating was applied to the side had electrical conductivity.

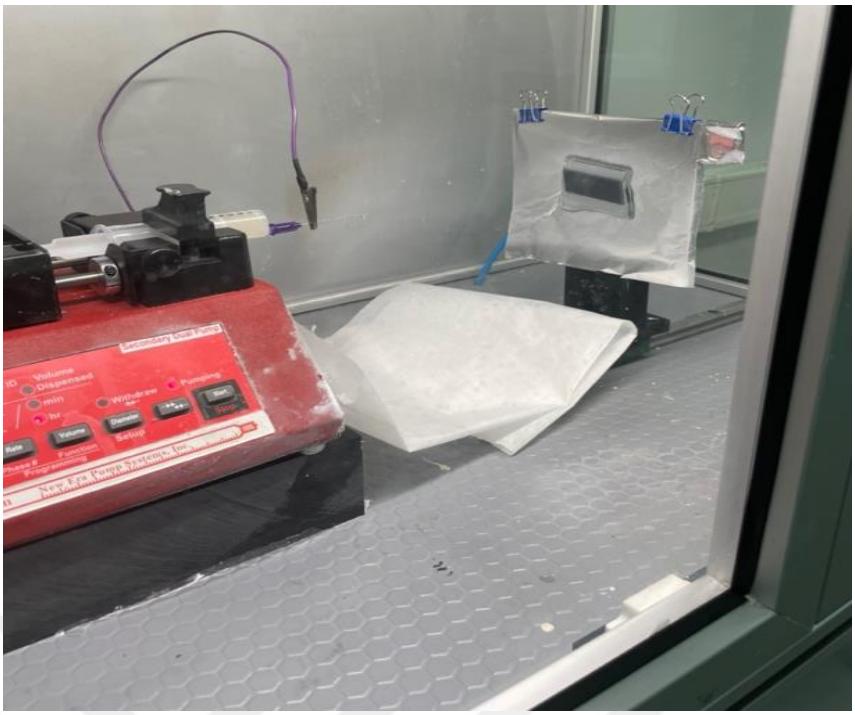

(a)

(b)

Figure 3.4: (**a**) Electrospinning device setup, (**b**) ITO glass affixed to aluminum foil with carbon tape.

Initially, 5 ml of solutions were drawn into syringe and the syringe was fixed to the electrospinning device. The variabes used in the electrospinning experiments are shown in Table 3.5 Distance in cm means distance between the needle and collector. The coating process of each solution on ITO glass (Figure 3.5) took about 1 h to get homogenous coating.

Table 3.5: Parameters of the Electrospinning

Parameters	Values
Needle Number (Gauges)	21
Needle Inner Diameter (mm)	0,51
Feed Rate(mL/hour)	5
Applied voltage (kV)	9
Distance between needle and the collector (cm)	15

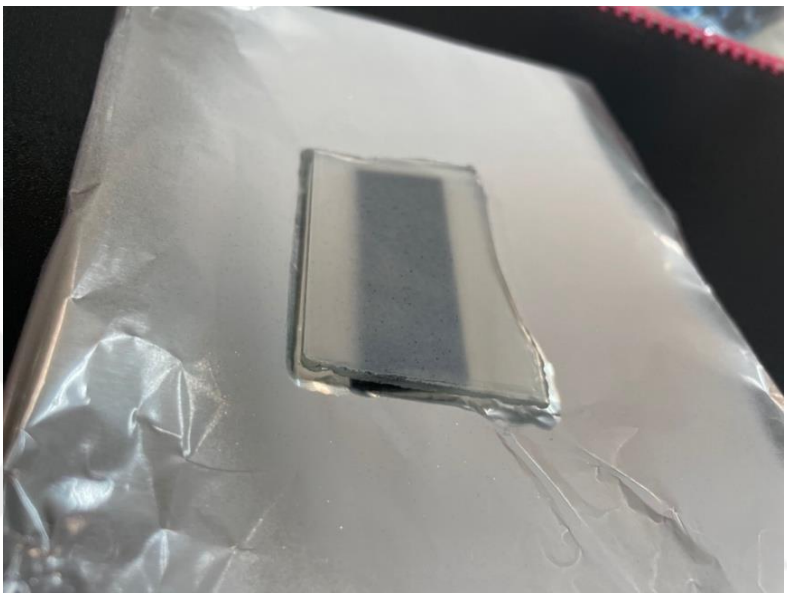

Figure 3.5: Thin film coating of nanofibers obtained from 10 wt.% Ag-PVA on ITO glass.

3.4 CHARACTERIZATION

3.4.1 Microstructural Characterization

The morphological structures and diameters of the produced fibers were determined using the SEM (Scanning Electron Microscopy) system (JSM 6335F – JEOL and JSM 6510LV – JEOL) at 10 kV in the laboratories of TUBITAK Marmara Research Center (TUBITAK MAM).

3.4.2 Determination of Nanofiber Size Distribution

The determination of fiber diameter was conducted using the "Image J" image analysis software. A total of 100 measurements were taken on SEM images for each sample to determine the average nanofiber diameter. Additionally, 20 measurements were taken to determine the average particle sizes. The obtained data were visualized into graphs using the "GraphPad Prism 9" graphing software.

3.4.3 Determination of Electrical Properties

Resistance values were determined by taking 20 measurements at various points on the ITO-coated glass using a "Rish Multi 18s" brand multimeter.

Thickness values were determined by taking 20 measurements from various regions of the samples coated with thin films using a "Mitutoyo Absolute" brand digital thickness measurement device as shown in Figure 3.6.

Figure 3.6: The thickness measurement setup

The average value of the 20 thickness measurements was obtained, and resistivity values were calculated by multiplying each resistance value with this average thickness value.

CHAPTER IV
RESULTS & DISCUSSION

In this part of the thesis, the microstructural examination, size distribution and the electrical properties, namely, resistance and the resistivity values are presented for coatings composed of fibers containing 3 and 5 wt.% nanoparticles. On the other hand, microstructure of fibers with 10 and 20 wt.% nanoparticles are not presented since too much agglomeration of nanoparticles were observed in the fibers. However, electrical resistance and resistivity of the coatings made up of 10 and 20 wt.% nanoparticles doped fibers are given for comparison.

4.1 MICROSTRUCTURAL EXAMINATION

4.1.1 Silver Doped Nanofiber Coatings

Figure 4.1 displays PVA nanofibers doped with 5 wt.% Ag nanoparticles. The diameters of the 5 wt.% Ag-PVA nanofibers were observed to change between 260 and 500 nm and had an average fiber diameter of around 380±48 nm (Figure 4.2), which was larger than the size of the nanoparticles. However, it has been observed that Ag nanoparticle distribution was not homogenous in the fibers and Ag nanoparticle agglomerated in some regions of the fibers. Compared to other nanoparticles used in the study, Ag nanoparticles exhibited higher degree of agglomeration during mixing stage, which lead to sedimentation of nanoparticles at the bottom of PVA solution and subsequent agglomeration in the produced nanofibers. As seen in Figure 4.3, the sizes of the agglomerated particles was between 2100 nm and 2700 nm. The agglomeration of nanoparticles on fibers is an undesirable condition. This condition indicates that the electrical resistance of Ag nanoparticles coated on ITO glass cannot be significantly reduced. The reduction in the concentration of added nanoparticle powders in the PVA solution can be employed to minimize the agglomeration on the fibers. Accordingly, PVA solution containing 3 wt.% Ag was electrospun to coat a thin film on ITO glass.

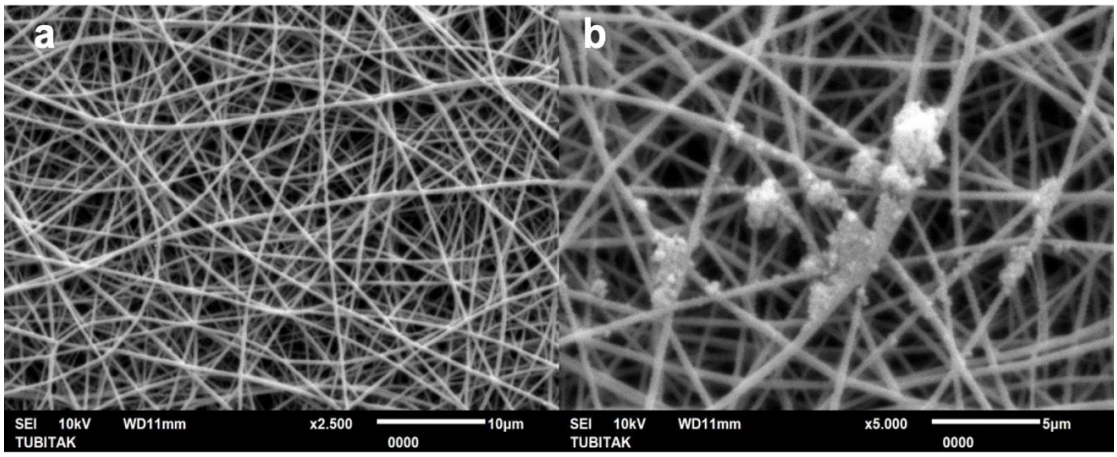

Figure 4.1: SEM image of the thin film coating obtained using 5 wt.% Ag – PVA solution. (a) x2.500 (b) x5.000

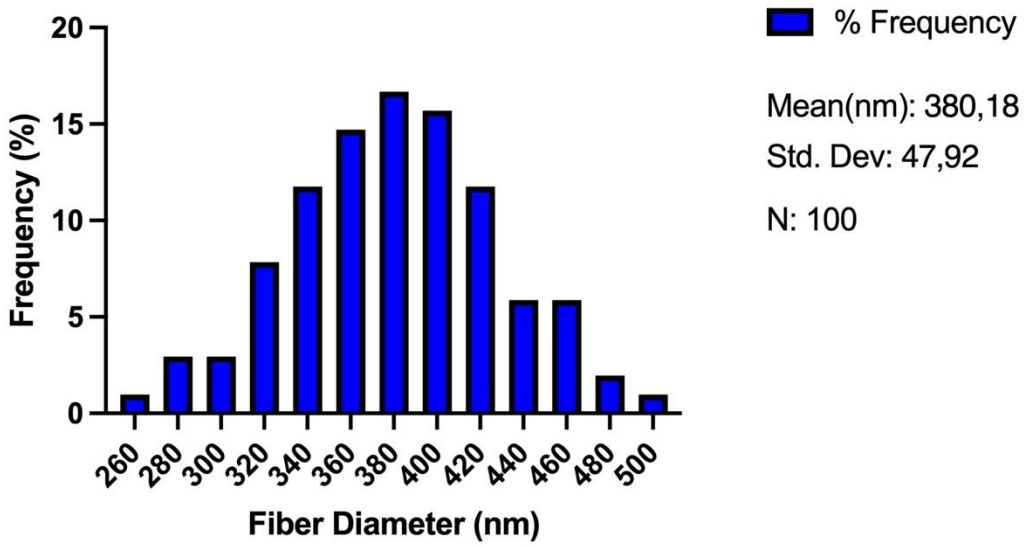

Figure 4.2: Comparison the resistance of thin films containing fibers with 5 wt.% nanoparticles

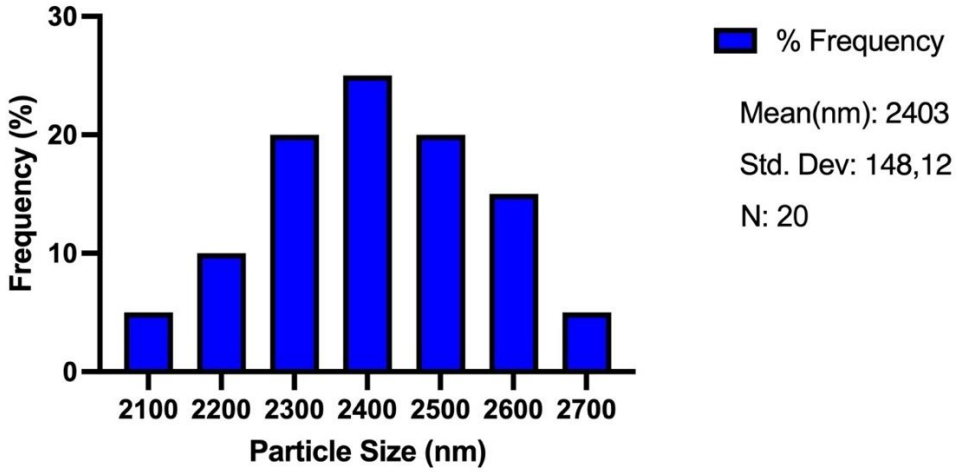

Figure 4.3: The frequency size distribution of agglomerated Ag nanoparticles in fibers obtained using 5 wt.% Ag – PVA solution.

As seen in Figure 4.4, decreasing the Ag nanoparticle content in PVA solution from 5 to 3 wt.%, reduced the agglomeration of nanoparticles in nanofibers. The reduction of Ag content in the solution had almost no effect on the resultant nanofiber diameter (Figure 4.5) and nanofibers displayed a diameter of around 377 ± 47 nm, which was close to diameters of fiber produced using 5 wt.%Ag-PVA solution. Because the PVA solution concentration was kept constant during each electrospinning experiment. As can be seen in Figure 4.6, average size of the agglomerated regions were 1554 nm, lower than the value (2403 nm) found in fibers produced using 5 wt.%Ag-PVA solution.

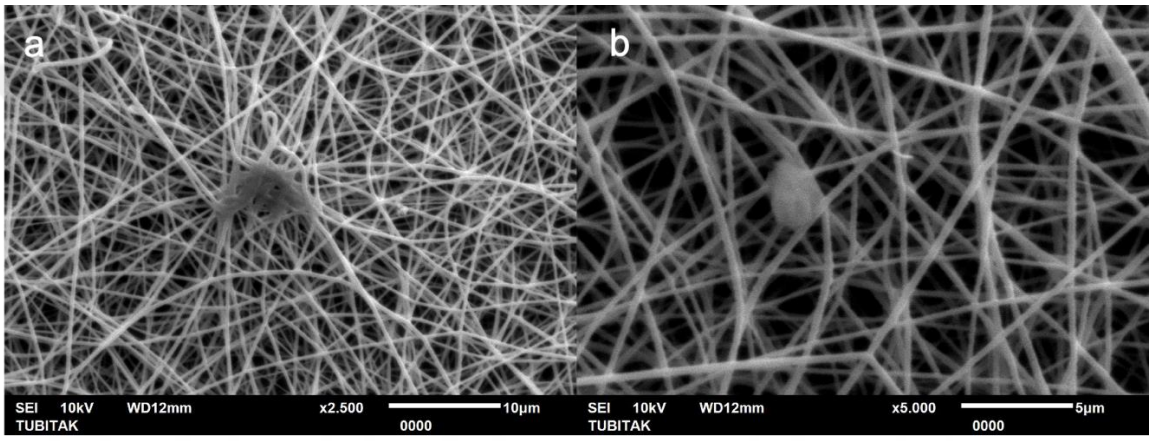

Figure 4.4: SEM image of the thin film coating obtained using 3 wt.% Ag – PVA solution. (a) x2.500 (b) x5.000

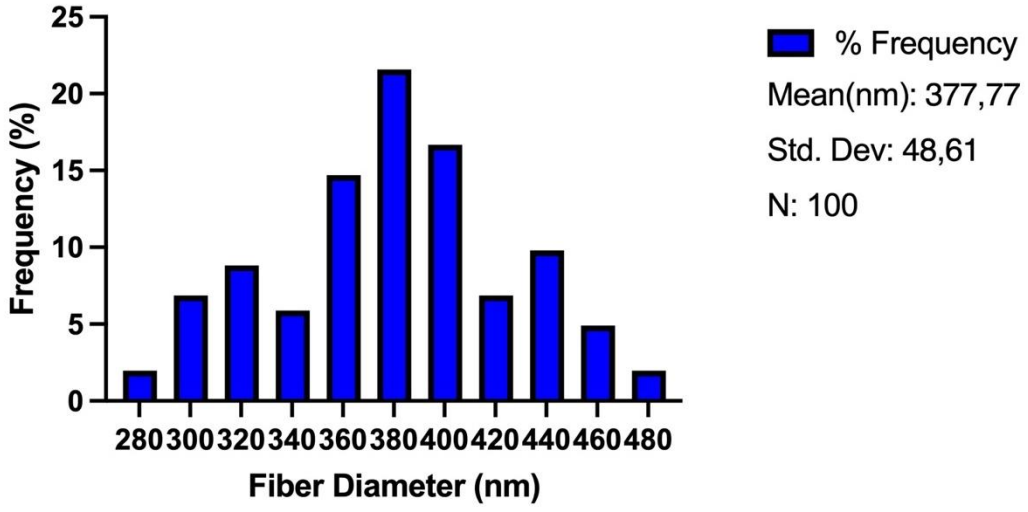

Figure 4.5: The frequency distribution of sizes of the fiber sizes obtained using 3 wt.% Ag – PVA solution.

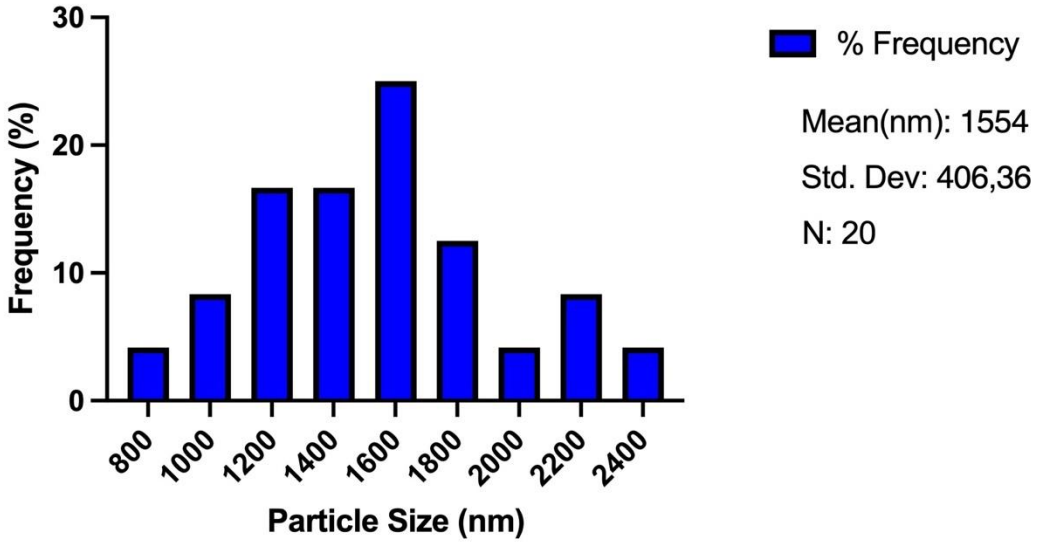

Figure 4.6: The frequency size distribution of agglomerated Ag nanoparticles in fibers obtained using 3 wt.% Ag – PVA solution.

4.1.2 ZnO Doped Nanofiber Coatings

Figure 4.7 shows the 5 wt.% ZnO doped nanofibers coated on ITO glass. The measured porosity content of the coating was around 32.5%. The diameter of the fibers was observed to change between 260 and 480 nm, with an average fiber diameter of 375 ± 46 nm. The average diameter of the fibers obtained using 5 wt.% ZnO-PVA solution was close to that of fibers obtained from 5 wt.% Ag-PVA solution since the concentration PVA solution in two cases was similar.

Similar to Ag nanoparticles doped in nanofibers, ZnO nanoparticles was found to agglomerate in some regions of the nanofibers. The agglomerated ZnO nanoparticle region size was around 3229 ± 418 nm in fiber ontained using 5 wt.% ZnO-PVA solution (Figure 4.9), which was higher compared to agglomerated nanoparticle region size (2403 nm) in fibers obtained 5 wt.% Ag-PVA solution. Although the density of ZnO (5.61 g/cm^3) is significantly lower than the density of silver (10.49 g/cm^3), agglomeration in ZnO nanoparticles was more severe which was attributed to the different surface chemistry.

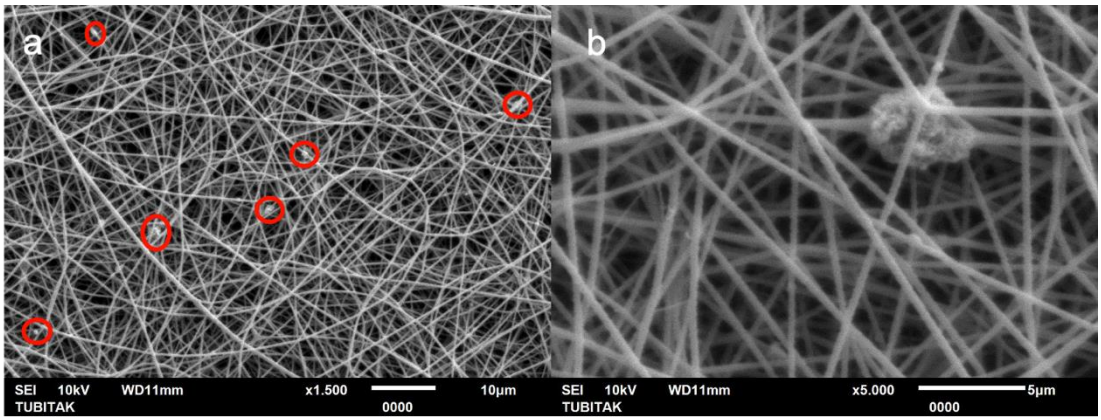

Figure 4.7: SEM image of the thin film coating obtained using 5 wt.% ZnO – PVA solution. (a) x1.500 (b) x5.000

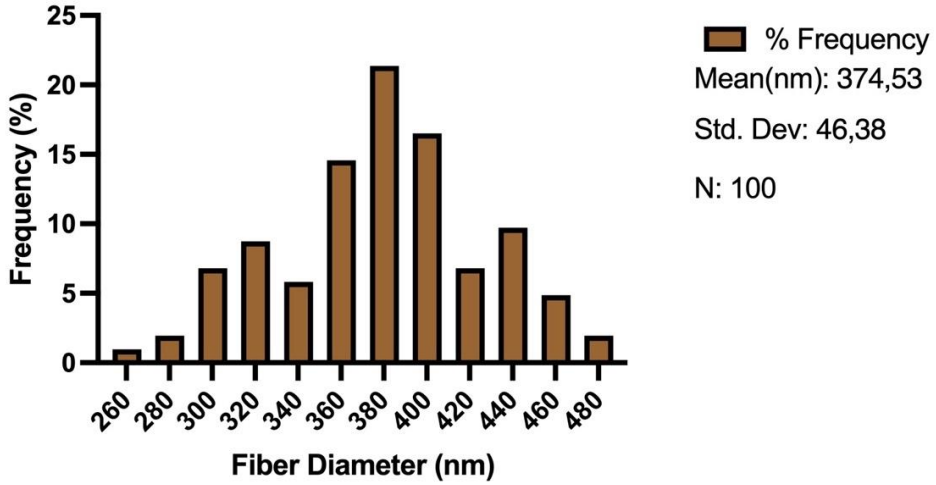

Figure 4.8: The frequency distribution of sizes of the fibers obtained using 5 wt.% ZnO – PVA solution.

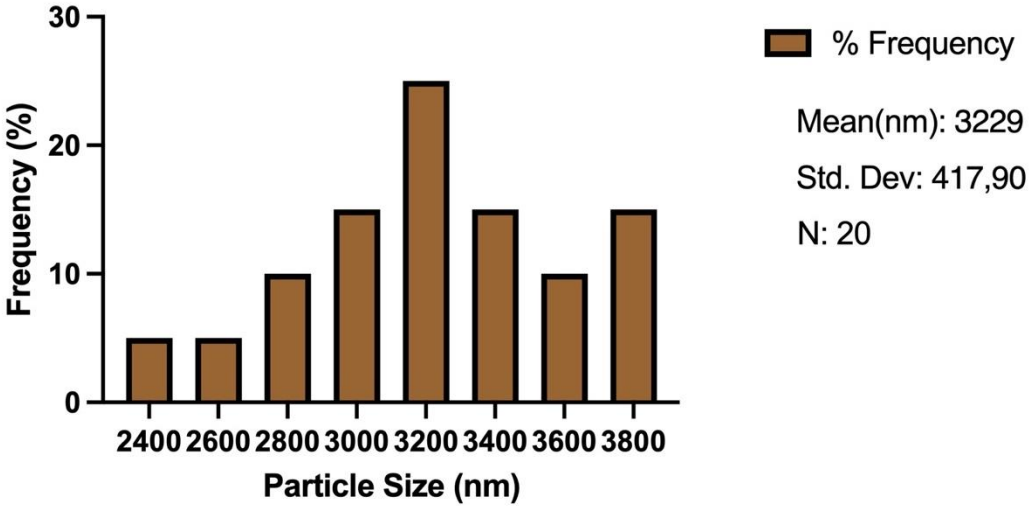

Figure 4.9: The frequency size distribution of agglomerated ZnO nanoparticles in fibers obtained using 5 wt.% ZnO – PVA solution.

Figure 4.10 shows nanofiber morphology obtained using 3 wt.% ZnO-PVA solution. As expected, nanofiber diameter remained almost contant (376 ± 48 nm, Figure 4.11) since the PVA solution was kept constant as in the previous experiments. However, upon decreasing the ZnO content from 5 to 3 wt.% in PVA solution decreased the agglomerated ZnO nanoparticle region size from 3229 ± 418 nm to 965±93 nm (Figure 4.12).

Similar to Ag nanoparticles, the degree and size of agglomeration in ZnO nanoparticles decrease as the nanoparticle concentration was reduced in PVA solution. However, while the average particle size decreased from 2403 nm to 1554 nm when Ag nano particle content was decreased from 5 to 3 wt.%, it decreased from 3229 nm to 965 nm when the change was made in ZnO content. This indicates that the effect of concentration ratio on the size of agglomeration in ZnO nanoparticles is greater than that that of Ag nanoparticles.

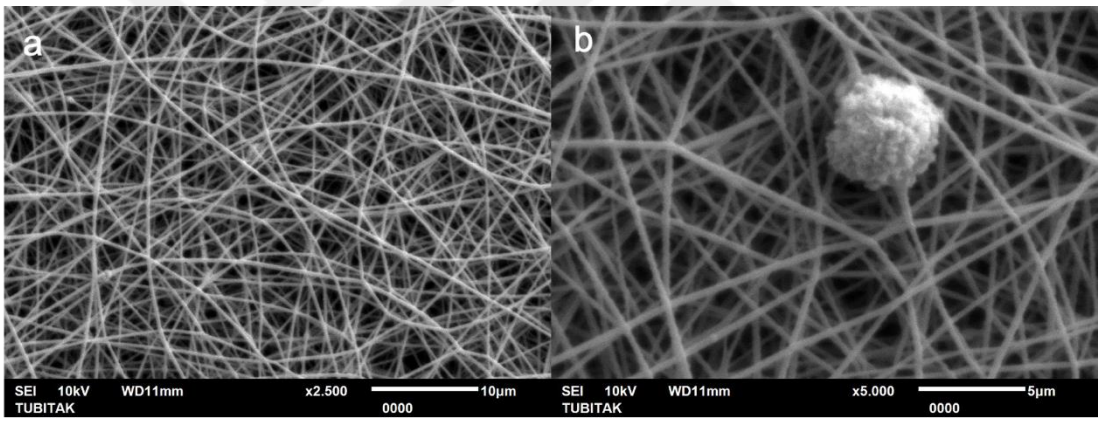

Figure 4.10: SEM image of the thin film coating obtained using 3 wt.% ZnO – PVA solution. (a) x2.500, (b) x5.000

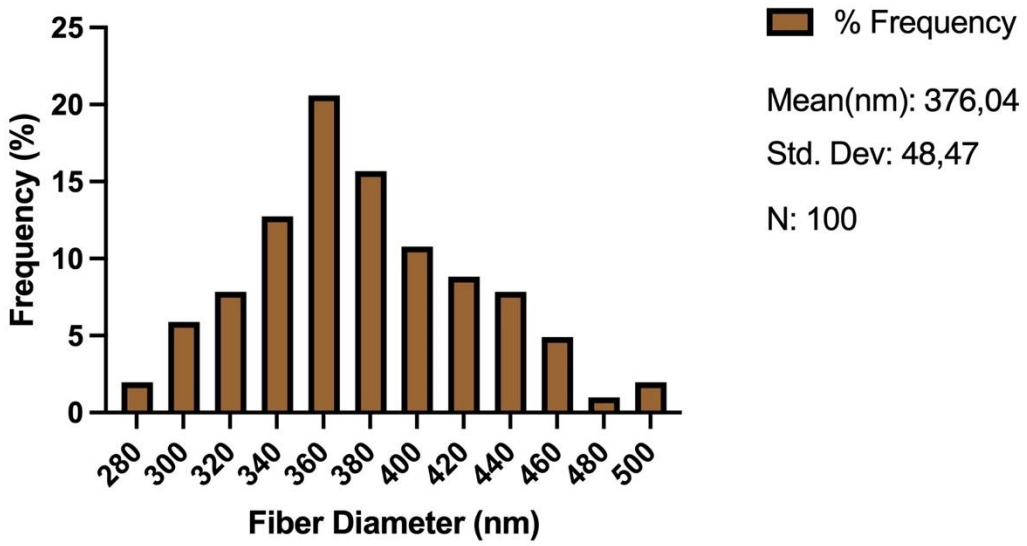

Figure 4.11: The frequency size distribution of nanofibers obtained using 3 wt.% ZnO – PVA solution.

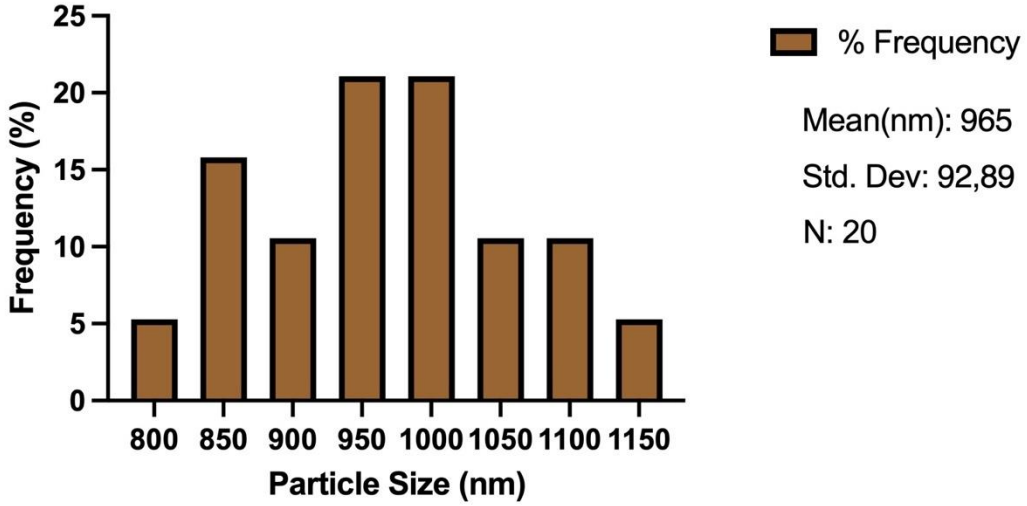

Figure 4.12: The frequency size distribution of agglomerated ZnO particles in fibers obtained using 3 wt.% ZnO – PVA solution.

4.1.3 TiO_2 Doped Nanofiber Coatings

Figure 4.13 displays coating and the morphology of nanofibers obtained using 5 wt.% TiO2-PVA solution. The porosity content of the coating was around 13.1%. On the other hand, the average fiber diameter was observed to change between 260 and 500 nm with an average fiber size of around 360±45 nm (Figure 4.14), which was close to diameter of nanofibers obtained using different dopants.

The average size of the agglomerated TiO2 regions was around 1242±144 nm smallest among all of the agglomerated nanoparticles (TiO2, Ag and ZnO) formed with the same dopant content. TiO2 nanoparticles provided the lowest aggregation on the fibers. Because, TiO_2 has lowest density (4.23 g/cm^3) compared to other in this experiment nanoparticles.

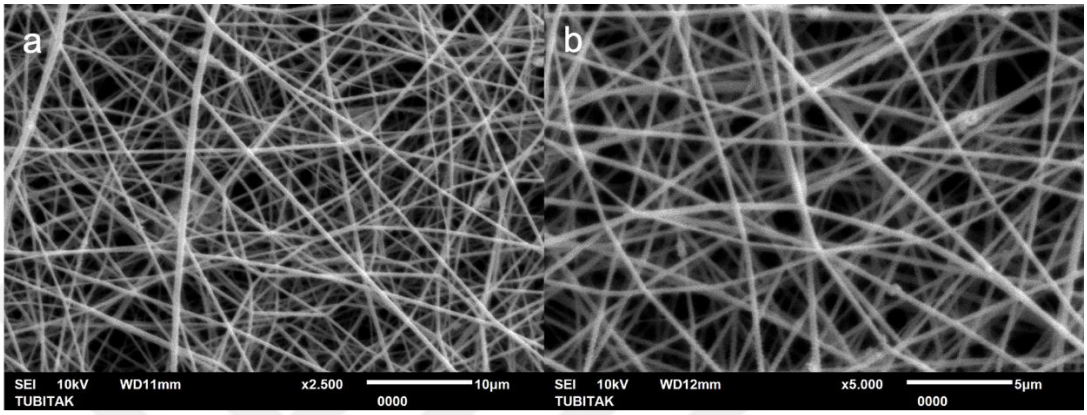

Figure 4.13: SEM image of the thin film coating obtained using 5 wt.% TiO_2 - PVA solution. (a) x2.500 (b) x5.000

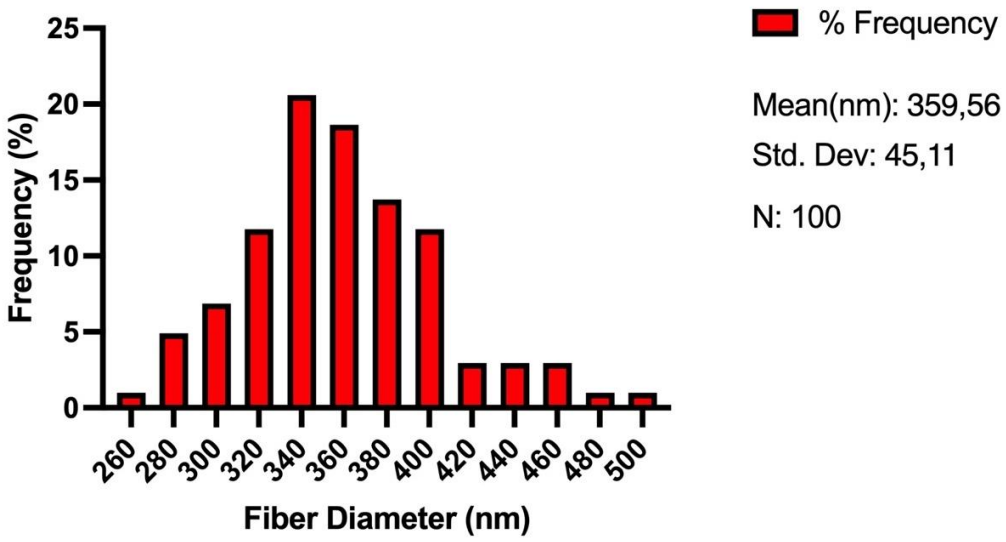

Figure 4.14: The frequency size distribution fiber sizes obtained using 5 wt.% TiO_2 - PVA solution.

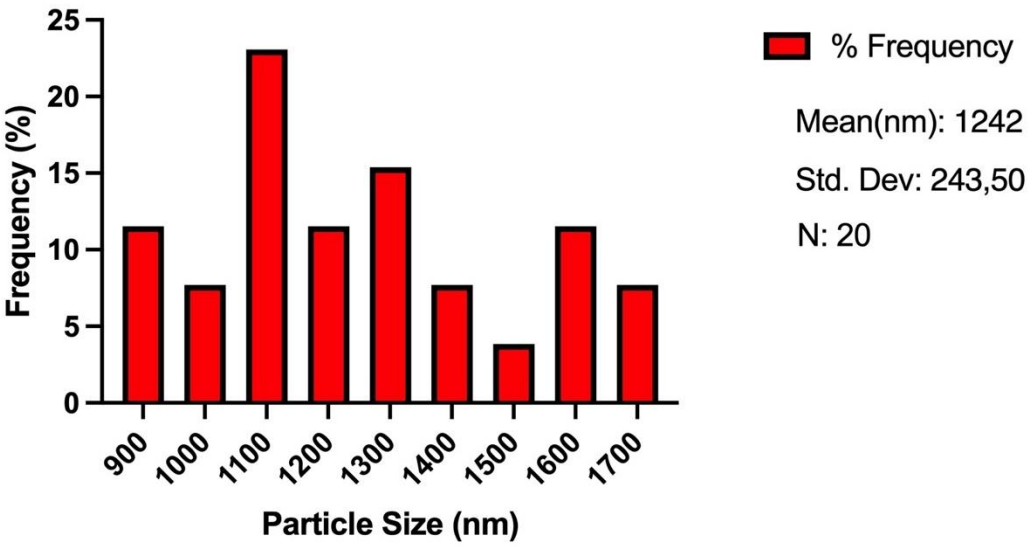

Figure 4.15: The frequency size distribution of agglomerated TiO_2 particles in fibers obtained using 5 wt.% TiO_2– PVA solution.

Figure 4.16 shows the morphology of coating and the fiber when TiO2 nano particle content was decreased form 5 to 3 wt.%. As expected, fiber diameter remained almost unchanged and the average fiber diameter was measured as 370±53 nm (Figure 4.17). On the other hand, decreasing the TiO2 content in PVA solution down to 3 wt.% decreased the agglomeration as well. The size of the agglomerated TiO2 region was around 644 nm in fibers (Figure 4.18), which was the smallest agglomerated size among all nanoparticles, where it was 1554 nm for 3 wt.% Ag-PVA solution and 965 nm for 3 wt.% ZnO-PVA solution, respectively.

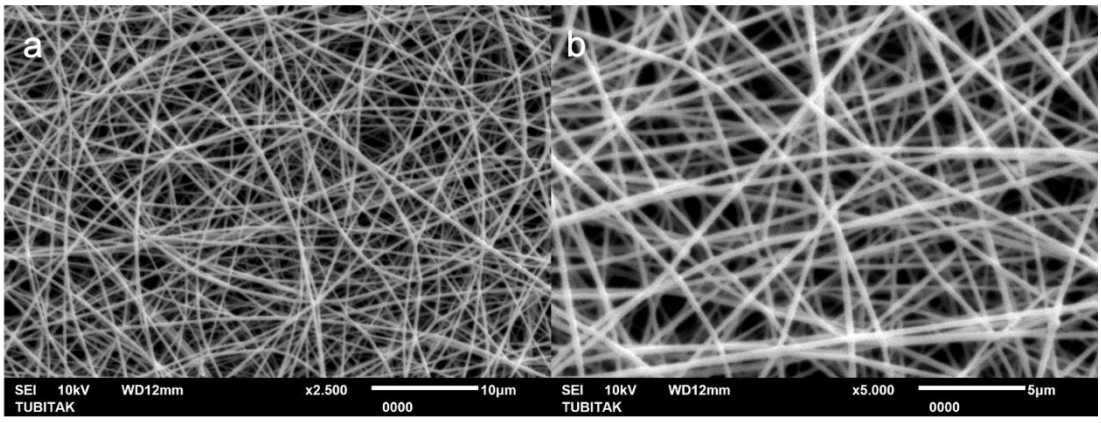

Figure 4.16: SEM image of the thin film coating obtained using 3 wt.% TiO_2 - PVA solution. (a) x2.500 (b) x5.000

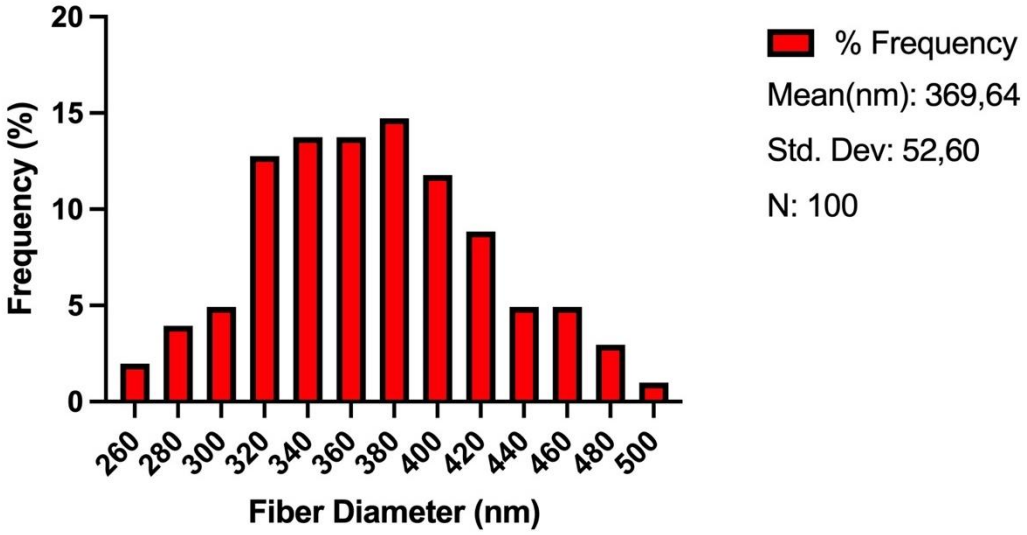

Figure 4.17: The frequency size distribution of nanofibers obtained using 3 wt.% TiO_2 - PVA solution.

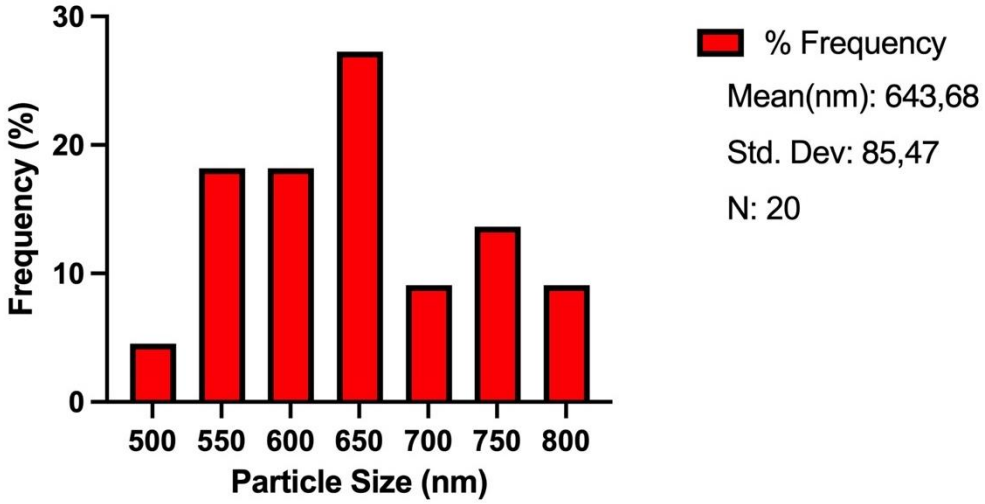

Figure 4.18: The frequency size distribution of agglomerated TiO2 particles in fibers obtained using 3 wt.% TiO – PVA solution.

The average size of agglomerated particles is 1554 nm for 3% wt Ag, 965 nm for 3% wt ZnO, and 643.68 nm for 3% wt TiO_2. It has been observed that TiO_2 has the least amount of agglomeration compared to Ag and ZnO when its microstructure is examined.

Based on the results obtained from the experiments, it was observed that thin fibers below 1000 nm were obtained using the electrospinning method. Due to same PVA solution (10 wt.%) utilized in electrospinning, the diameters of the fibers were

similar to each other. However, slightly higher diameter was detected for the Ag doped nanofibers for all dopant concentrations, i.e. 5 and 3 wt.% (Table 4.1), while the smallest diameter was observed in TiO_2 doped nanofibers. Although the added nanoparticle size were all around 100 nm, slightly different nanofiber diameter was obtained in fibers doped with different nanoparticles. As mentioned in the previous parts, there is no correlation between the density of nanoparticles and fiber diameters. The reason of such difference was attributed to surface chemistry and surface energy of nanoparticles, which influence the homogenous distribution in the solution and viscosity of the solurion as well. As described in previous studies, maintaining a Tip-to-Collector Distance at 15 cm also prevented bubbling on the fibers [79].

In studies conducted on electrospinning, the average diameter of TiO_2/PVA nanofibers was reported as 367.3 nm for 3 wt. % TiO_2 added PVA [97]. In another study, it was noted that fibers with doped with 5 wt. % TiO_2 and ZnO nanoparticles had diameters mostly ranging between 300-400 nm [98]. The diameters of the fibers produced in the present study are found to be similar to diameter of fibers synthesized in other studies. However, the reason of diameter change with the type of nanoparticles should be explored and clearified to other studies.

Table 4.2 displays the size of agglomerated nanoparticle regions with respected to added nanoparticle amount to PVA solution. As can be seen, there is a correlation between nanoparticle content in PVA solution and the size of agglomerated regions. The size of the agglomerates tended to decrease as the added nanoparticle content decreased possibly due to more distribution of nanoparticles at lower concentration. However, an extra step is needed to get homogenous distribution of nanopowders in PVA solutions, which include surface engineering and changes the surface chemistry of nanoparticles. On the other hand, there were no direct correlation between the type of nanoparticle and the the size of agglomerates; however, the smallest degree of agglomeration was observed TiO_2 added fibers. Therefore, among the used nanoparticles, TiO_2 was the most suitable nanoparticle in terms of produced thinner fibers and least agglomeration observed

Table 4.1: Mean diamaters of fibers of produced electrospinning of PVA solutions with different nanoparticle (NP) contents.

Type of Nanoparticles	Mean of Fiber Diameters	
	5 wt.% NP-PVA solution	3 wt.% NP-PVA solution
Ag	380.2±47.9 nm	377.7±48.6 nm
ZnO	374.5 ± 46.4 nm	376.0 ± 8.5 nm
TiO_2	359.6 ± 45.1 nm	369.6 ± 52.6 nm

Table 4.2: Size of agglomarated nanoparticles at different nanoparticle (NP) content

Type of Nanoparticles	Size of Agglomerated Nanoparticles	
	5 wt.% NP-PVA solution	3 wt.% NP-PVA solution
Ag	2403 ± 148.1 nm	1554 ± 406.4 nm
ZnO	3229 ± 417.9 nm	965 ± 92.9 nm
TiO_2	1242 ± 243.5 nm	643.7 ± 85.5 nm

4.2 ELECTRICAL PROPERTIES

In this section of the thesis, both sheet resistance and the resistivity of the thin films containing nanoparticle doped fibers are presented. In order to determine the resistance of the ITO glasses coated with electrospun films, 20 different measurements were taken from various regions of the glass. The resistance of the ITO glass was measured to be 34 ohms in each region, and this value was entered to corresponding resistance values of the 20 samples obtained.

The resistivity of the thin films were calculated by multiplication of the average sheet resistances with the average thickness of the thin film obtained from thickness measurements taken form 20 different points.

Table 4.4 and Table 4.5 display the mean resistance and resistivity values of thin film coatings on ITO glass which are composed nanoparticle doped fibers. As can be seen, the resistance and the resistivity of thin films are influenced from both the content and the type of nanoparticles. It has been seen that the resistance and the resistivity values of coatings decreased as the content of nanoparticles decreased, possibly due to less degree agglomeration when there was low amount of nanoparticles. However, for the coatings with fiber containing Ag nanoparticles over 10 wt.% displayed different behaviour. Severe agglomeration over 10 wt.% addition of nanoparticles may be the reason of such behavior.

For high conductivity, thin film coating with low resistance and resistivity is desired. Therefore, the point, where the ITO glass resistance, 34 Ω, has been reached, is critical to for evaluation of effectiveness of the coatings. For the coatings containing Ag and ZnO nanoparticles, the resistance reached to resistance of ITO glass when concentration of nanoparticles decreased down to 5 wt.%. On the other hand, coatings with TiO_2 particles, resistance of the coating became equivalent to that of ITO glass at 10 wt.% addition. Lower resistance of TiO_2 containing thin film coatings was attributed to lower degree of agglomeration of nanoparticles as shown in previous section. The resistivity values of the coatings given in Table 4.5 showed similar trend since the resistivity was calculated by multiplication of film thickness by film resistance.

Table 4.3 shows the average thickness values of ITO glass after coating which are composed nanoparticle doped fibers. No correlation was observed between nanoparticle concentration and the thicknesses of ITO glass. Additionally, no correlation was observed with changes in electrical properties. This is because the concentration of the coating polymer solution and the coating parameters during electrospinning were kept constant.

Table 4.3: Mean of thickness at different wt.% thin films composed of fibers produced electrospinning of PVA solutions with different nanoparticle (NP) contents.

Type of Nanoparticles	**Mean of Thickness, (mm)**			
	20 wt.% NP-PVA solution	10 wt.% NP-PVA solution	5 wt.% NP-PVA solution	3 wt.% NP-PVA solution
Ag	2.248	2.260	2.313	2.266
ZnO	2.253	2.252	2.285	2.302
TiO_2	2.248	2.248	2.290	2.291

Table 4.4: Mean of resistance at different wt.% thin films composed of fibers produced electrospinning of PVA solutions with different nanoparticle (NP) contents.

Type of Nanoparticles	**Mean of Resistance, R (Ω)**			
	20 wt.% NP-PVA solution	10 wt.% NP-PVA solution	5 wt.% NP-PVA solution	3 wt.% NP-PVA solution
Ag	32.83	46.56	33.85	31.80
ZnO	47.66	44.78	34.09	33.09
TiO_2	37.44	33.35	31.97	30.83

Table 4.5: Mean of resistivity of thin films composed of fibers produced electrospinning of PVA solutions with different nanoparticle (NP) contents.

Type of Nanoparticles	**Mean of Resistivity, ρ (Ωmm)**			
	20 wt.% NP-PVA solution	10 wt.% NP-PVA solution	5 wt.% NP-PVA solution	3 wt.% NP-PVA solution
Ag	738.05	1052.16	782.79	720.82
ZnO	1074.09	1008.44	779.15	761.70
TiO_2	834.63	749.67	732.09	706.52

As it is seen in Tables 4.4 and 4.5, in addition to content of nanoparticles, the type of nanoparticle effective on resistance and resistivity. Since severe agglomeration was detected for films containing 10 and 20 wt.% nanoparticle, the effect of nanoparticle type on electrical properties was discussed only for 3 and 5 wt.% nanoparticle additions. Figures 4.19 - 4.22 display resistance and resistivity change of films with respect to type of nanoparticles for 3 and 5 wt.% addition. At 5 wt.% nanoparticle addition, the coatings with Ag and ZnO nanoparticles showed comparable resistance to that of ITO glass (Figure 4.19). On the hand, addition of same amount of TiO2 doping resulted around 32 Ω resistance, below the ITO resistance. Although the conductivity of Ag is higher than other nanoparticles, Ag doped coating displayed resistance to those containing ZnO particles. The reason comperatively high resistance values of film with Ag nanoparticles was possibly due to agglomeration. However, upon decreasing the content of Ag nanoparticle down to 3 wt.% caused decreasing of the resistance (Figure 4.21). The resistance decreased to around 32 Ω, below the ITO glass value. Decreasing the Ag content lowered the agglomeration degree in Ag nanoparticles, therefore, Ag particles effectively increased the conducitivity (Figure 4.22).

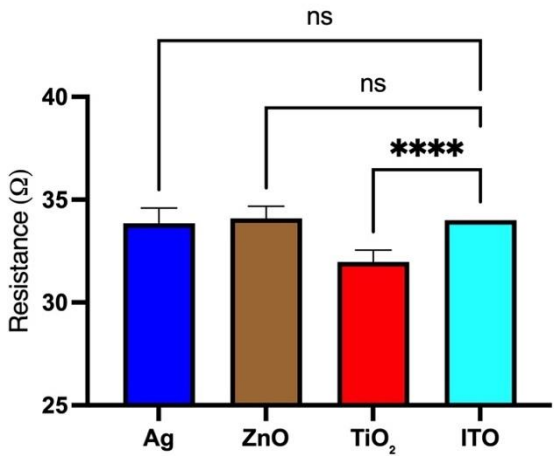

Figure 4.19: Comparison of the resistances of ITO glass and films containing 5 wt.% nanoparticle.

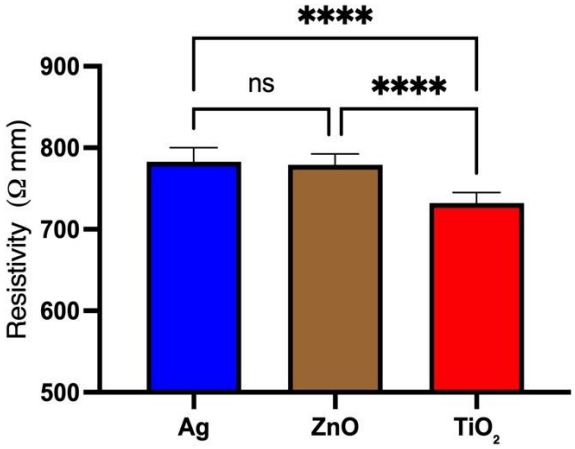

Figure 4.20: Comparison of the resistivity of films containing 5 wt.% nanoparticle.

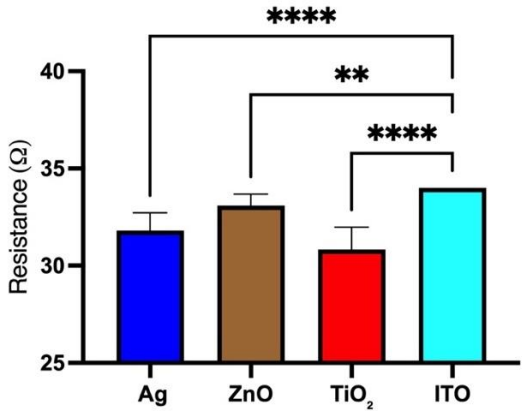

Figure 4.21: Comparison of the resistances of ITO glass and films containing 3 wt.% nanoparticle.

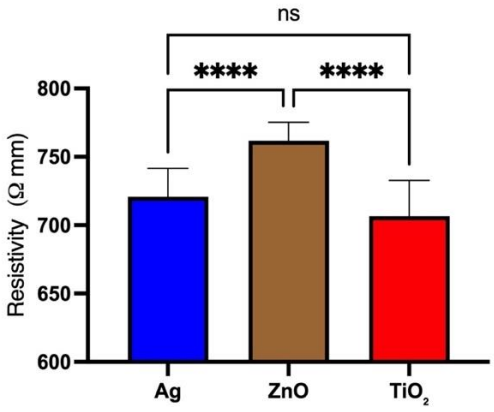

Figure 4.22: Comparison of the resistivity of films containing 3 wt.% nanoparticle.

Table 4.6 shows the studies in the literature aimed at improving the electrical properties of ITO glass, including the coating methods, coated materials, and obtained results. F. Švegland et. al managed to reduce the resistivity value to 1.9×10^{-1} by coating Co3O4 on ITO glass using the sol-gel method at 300 °C[99]. T. Mohammad et. al managed to reduce the resistivity value to 5.9×10^{-2} by coating Eu3+ doped Poly (3,4-ethylenedioxythiophene):poly(styrene sulfonate) (PEDOT:PSS) on ITO glass using the spray deposition method at 1kV [100]. H. Taha et. al successfully reduced the resistivity value to 5.8×10^{-4} by coating Ag on ITO glass using the sol-gel method at 500 degrees[101].

The resistivity values obtained in the thesis study were observed to be higher compared to the literature. This is due to the different types of coating methods used on ITO glass in the literature. As can be seen from the SEM images of the coatings made on ITO glass using the electrospinning method, a porous structure was observed in the surface morphology of the coatings. Therefore, the resistivity values may have been affected by the presence of the porous structures on the coatings.

Table 4.6: Results of studies in the literature on improving the electrical properties of ITO coatings

Type of Material Coated	Coating Method	Resistiviy (Ωcm)
Co_3O_4	Sol-Gel	1.9×10^{-1}
Eu^{3+}	Spray Deposition	5.9×10^{-2}
Ag	Sol-Gel	5.8×10^{-4}

CHAPTER V
CONCLUSION

In this thesis study, thin film coatings were formed on ITO glass by electrospinning of Ag, ZnO, and TiO_2 nanoparticles doped PVA solution. Following conclusions have been drawn at the end of this study:

1- Electrospinning of nanoparticle doped PVA solution resulted in the formation of porous thin films on ITO glasses. The porosity of the thin films reached up to 32.5% in ZnO doped films, in which the highest degree of particle agglomeration was observed at 5 wt.% addition. On the other hand, TiO_2 containing films exhibited lowest porosity, i.e. ~13%, possibly because of lesser degree of agglomeration.

2- Nanoparticles were observed to agglomerate in fibers and the size of the agglomerated regions become larger by increasing the nanoparticle content. Agglomeration was found to be independent from density of nanoparticles at nanoparticle concentrations above 5 wt.%.

3- At low nanoparticle concentration of 3 wt.%., there was a direct relationship between size of agglomerates and the density of Ag (10, 49 g/cm^3), ZnO (5.61 g/cm^3) and TiO_2 (4.23 g/cm^3) nanoparticles. The size of the agglomerated regions were 1554 ± 406.4 nm, 965 ± 92.9 nm and 643.7 ± 85.5 nm for Ag, ZnO and TiO_2 nanoparticles, respectively.

4- Smallest fiber diameter of 359.6 ± 45.1 nm was obtained using solution containing 5 wt.% TiO_2 nanoparticles.

5- The resistance and the resistivity values decreased by decreasing the content of nanoparticles due to decreased agglomeration. For the TiO_2 doped fiber containing film, in which there is more homogenous distribution in fiber sizeand less agglomeration, the resistance became equilivalent to resistance of

6- ITO glass (34 Ω) at 10 wt.% TiO_2 addition, below which the resistance of the thin film decreased more.
7- For the thin films containing fiber doped with ZnO and Ag nanoparticles, ITO resistance value was reached only when the nanoparticle content decreased down to 5 wt.%. Relatively severe agglomeration of ZnO and Ag nanoparticles increased the resistivity of thin films.

CHAPTER VI
FUTURE STUDIES

1- Addition of nanoparticles to PVA solution resulted in agglomeration and it was partly prevented by increasing the magnetic stirring time. However, surface chemistry of the nanoparticles should be changed to create electrostatic repulsion or steric hinderence in nano powders by using different techniques of surface engineering for prevention of agglomeration during fiber production.

2- A detailed investigation should be conducted to reveal the reason of less agglomeration observed in TiO_2 nanoparticles.

3- A detaled TEM study should be conducted to examine the nanoparticles morphology doped in PVA fibers.

4- Four point probe method should be used to determine sheet resistance and the resistivity of the thin films.

REFERENCES

[1] TEKO Ahmet (2014), *Saydam iletken oksit tabakalarda yapısal özelliklerin araştırılması* (Master Thesis), Yıldız Technical University, İstanbul.

[2] KIM Jun Kwan, YUN Sun Jin, LEE Jae Min, and LIM Jung Wook (2010), "Effect of RF-power density on the resistivity of Ga-doped ZnO film deposited by RF-magnetron sputter deposition technique", *Current Applied Physics*, vol. 10, pp. 451-454.

[3] BEYER Wolfhard, HUPKES Jürgen, and STIEBIG Helmut (2007), "Transparent conducting oxide films for thin film silicon photovoltaics", *Thin Solid Films*, vol. 516, pp. 147-154.

[4] STADLER Andreas (2012), "Transparent conducting oxides-An up-to-date overview", *Materials*, vol. 5, pp. 661-683.

[5] BEZIR Nalan and EVCIN Atilla (2013), "Ag katkılı TiO2 nanofiberlerin üretim ve karakterizasyonu", *Afyon Kocatepe University Journal of Science and Engineering*, vol.14, no. 3, pp. 315-318.

[6] EREL Şerafettin and YILDIZ Kerem (2022), "Dye-Sensitized Solar Cells Based on Hybrid Photoanodes Consisting of ZnO Nanorods Embedded in TiO2 Nanoparticles", *Journal of Electronic Materials* , vol.51, no.11, pp.6188-6195.

[7] SAMPAIO Priscila Gonçalves Vasconcelos and GONZALES Mario Orestes Aguirre (2017), "Photovoltaic solar energy: Conceptual framework", *Renewable and Sustainable Energy Reviews*, vol. 74, pp. 590-601.

[8] GUL Mehreen, KOTAK Yash and MUNEER Tariq (2016), "Review on recent trend of solar photovoltaic technology", *Energy Exploration & Exploitation*, vol.34, pp 485-526.

[9] SAWLE Yashwant (2021), "Techno-economic comparative assessment of an off-grid hybrid renewable energy system for electrification of remote area", *In, Advances in Nonlinear Dynamics and Chaos (ANDC)*, Eds. Ahmad Taher Azar and Nashwa Ahmad Kamal, Academic Press, New York, pp. 199-247.

[10] WANG Aihua, ZHAO Jianhua, and GREEN Martin (1990), "24% efficient silicon solar cells", *Applied Physics Letters*, vol. 57, no. 6, pp. 605-607.

[11] SHAH Arvind, VANECEK Milan, MEIER Janne, VALLAT Evelyne, WYRSCH Nicolas and DROZ Corinne (2004), “Thin-film Silicon Solar Cell Technology”, *Progress in Photovoltaics: Research and Applications*, vol. 12, no. 2-3, pp 113-142.

[12] SHI Donglu, GUO Zizheng and BEDFORD Nick (2015) , “Nanoenergy materials”, *In, Nanomaterials and Devices*, Elsevier, New York, pp. 255-291.

[13] KARZAZI Yasser and ARBOUCH IMANE (2014), "Inorganic photovoltaic cells: Operating principles, technologies and efficiencies - review", *Journal of Materials and Environmental Science*, vol. 5, pp. 1505-1515.

[14] KIM Sanng Yong and CHUNG Jin Woong (2013), "Remarkable progress in thin-film silicon solar cells using high-efficiency triple-junction technology", *Solar Energy Materials and Solar Cells*, vol. 119, pp. 26-35.

[15] GREEN Martin, EMERY Keith, and HISHIKAWA Yoshihiro (2013), "Solar cell efficiency tables (version 42)", *Progress in Photovoltaics: Research and Application*, vol. 21, pp. 827-837.

[16]BAGHER Askari Mohammad, VAHID Mirzaei Mahmoud Abadi, and MOHSEN Mirhabibi (2015), "Types of solar cells and application", *American Journal of Optics and Photonics*, vol. 3, pp. 94-113.

[17] DAMBHARE Mugdha, BUTEY Bhavana, and MOHARIL Sanjiv (2021), "Solar photovoltaic technology: A review of different types of solar cells and its future trends", *Journal of Physics: Conference Series*, vol. 1913, no. 012053.

[18] HASHMI Syed and MIETTUNEN Kati (2011), "Review of materials and manufacturing options for large area flexible dye solar cells", *Renewable and Sustainable Energy Reviews*, vol. 5-6, pp. 3717-3732.

[19] GONG Jiawei and LIANG Jing (2012), "Review on dye sensitized solar cells (DSSCs): Fundamental concepts and novel materials", *Renewable and Sustainable Energy Reviews*, vol.16, pp. 5848-5860.

[20] ZATIROSTAMI Ahmad (2020), "A new electrochemically prepared composite counter electrode for dye-sensitized solar cells", *Thin Solid Films*, vol. 701, pp. 137926.

[21] PANIGRAHI Shrabani and BASAK Durga (2011), "Morphology driven ultraviolet photosensitivity in ZnO-CdS composite", *J. Colloid Interface Sci.*, vol. 364, pp. 10-17.

[22] ROBEL István, SUBRAMANIAN Vaidyanathan, KUNO Masaru and KAMAT Prashant (2006), "Quantum dot solar cells: Harvesting light energy with CdSe nanocrystals molecularly linked to mesoscopic TiO2 films", *J. Am. Chem. Soc.*, vol. 128, no. 7, pp. 2385-2393.

[23] PLASS Robert, PELET Serge, KRUEGER Jessica, GRAETZEL Michael and BACH Udo (2002), "Quantum dot sensitization of organic-inorganic hybrid solar cells", *J. Phys. Chem.*, vol. 106, pp. 7578-7580.

[24] YU Pingrong, ZHU Kai, NORMAN Andrew, FERRERE Suzanne, FRANK Arthur and NOZIK Arthur (2006), "Nanocrystalline TiO2 solar cells sensitized with InAs quantum dots", *J. Phys. Chem.*, vol. 110, pp. 25451-25454.

[25] KIM Hui-Seon, IM Sang Hyuk and PARK Nam-Gyu (2014), "Organolead halide perovskite: New horizons in solar cell research", *J. Phys. Chem*., vol. 118, pp. 5615-5625.

[26] ÜNLÜ Feray, JUNG Eunhwan, HADDAD Jinane, KULKARNI Ashish, OEZ Senol, CHOI Heechae, FISCHER Thomas, CHAKRABORTY Sudip, KIRCHARTZ Thomas and MATHUR Sanjay (2020), "Understanding the interplay of stability and efficiency in A-site engineered lead halide perovskites", *APL Materials*, vol. 8, no. 7, DOI: 10.1063/5.0011851.

[27] ASKIN Neslihan (2023), *Yüksek verimli perovskit güneş modüllerinin geliştirilmesi* (Master Thesis), Gebze Technical University, Kocaeli.

[28] PARK Nam-Gyu (2015), "Perovskite solar cells: An emerging photovoltaic technology", *Materials Today*, vol. 18, no. 2, pp. 65-72.

[29] GREEN Martin, HO-BAILLIE Anita and SNAITH Henry (2014), "The emergence of perovskite solar cells", *Nat. Photonics*, vol. 8, no. 7, pp. 506-514.

[30] MOHARRAM Khaled, ABD-ELHADY Mohamed, KANDIL Hamdy and EL-SHERIF Hisham (2013), "Enhancing the performance of photovoltaic panels by water cooling", *Ain Shams Eng. J*., vol. 4, no. 4, pp. 869-877.

[31] ABD-ELHADY Mohamed and FOUAD Mennatallah (2016), "Improving the efficiency of photovoltaic (PV) panels by oil coating", *Energy Convers. Manag*., vol. 115, pp. 1-7.

[32] MERAL Mehmet Emin, and DİNÇER Furkan (2011), "A review of the factors affecting operation and efficiency of photovoltaic based electricity generation systems", *Renew. Sustain. Energy Rev.*, vol. 15, no. 5, pp. 2176-2184.

[33] TRIPANAGNOSTOPOULOS Yiannis (2002), "Hybrid PV/T system with improved air heat extraction modification", *Proc. PV in Europe*, pp. 1-4, Rome.

[34] GARDAS Bhaskar, and TENDOLKAR Mandar (2012), "Design of cooling system for photovoltaic panel for increasing its electrical efficiency", *Proc. ICMIE*, pp. 144-149, Goa.

[35] PANDEY Adarsh Kumar, TYAGI Vineet Veer, SELVARAJ Jeyraj, RAHIM Nasrudin Abd, and TYAGI Sudhir Kumar (2016), "Recent advances in solar photovoltaic systems for emerging trends and advanced applications", *Renew. Sustain. Energy Rev.*, vol. 53, pp. 859-884.

[36] KALOGIROU Soteris (2013), *Solar Energy Engineering: Processes and Systems*, Academic Press, USA.

[37] GREEN Martin, EMERY Keith, HISHIKAWA Yoshihiro, WARTA Wilhelm, and DUNLOP Ewan (2015), "Solar cell efficiency tables (Version 45)", *Progress Photovolt: Res. Appl.*, vol. 23, no. 1, pp. 1-9.

[38] VIITANEN Janne (2015), *Energy efficient lighting systems in buildings with integrated photovoltaics* (MasterThesis), Aalto University,Espoo.

[39] COOK Gary, BILLMAN Lynn, and ADCOCK Rick (1995), *Photovoltaic Fundamentals*, National Renewable Energy Laboratory, USA.

[40] HOU Jianhui, PARK Mi-Hyae, ZHANG Shaoqing, YAO Yan, CHEN Li-Min, LI Juo-Hao, and YANG Yang (2008), "Bandgap and molecular energy level control of conjugated polymer photovoltaic materials based on benzo [1, 2-b: 4, 5-b′] dithiophene", *Macromolecules*, vol. 41, no. 16, pp. 6012–6018.

[41] BELLINGHAM J. R., PHILLIPS W. A., and ADKINS C. J. (1992), "Electrical and optical properties of thin films of F-doped SnO2 produced by spray pyrolysis", *J. Mater. Sci. Lett.*, vol. 11, p. 263.

[42] CHEN Meng, PEI Zhiliang, WANG Xi, SUN Cao, and WEN Lishi (2000), "Deposition and characterization of transparent conductive oxide ZnO: Al films prepared by direct current magnetron sputtering", *J. Phys. D: Appl. Phys*., vol. 33, p. 2538.

[43] SHIMIZU Makoto, SUZUKI Mari, IGUCHI Fumitada and YUGAMI Hiroo (2014), "High-temperature solar selective absorbers using transparent conductive oxide coated metal", *Energy Procedia*, vol. 57, pp. 418–426.

[44] KANG Dong-Won, CHOWDHURY Amartya, SICHANUGRIST Porponth, ABE Yusuke, KONISHI Hirofumi, TSUDA Yuki, SHINAGAWA Tomohiro, TOKIOKA Hidetada, FUCHIGAMI Hiroyuki, and KONAGAI Makoto (2015), "Highly transparent Zn1-xMgxO/ITO multilayer for window of thin film solar cells", *Current Applied Physics*, vol. 15, no. 9, pp. 1022-1026, DOI: 10.1016/j.cap.2015.05.017.

[45] GORDON Roy (2000), "Criteria for Choosing Transparent Conductors", *MRS Bull*., vol. 25, no. 8, pp. 52-57.

[46] GRANQVIST Claes (2007), "Transparent Conductors as Solar Energy Materials: A Panoramic Review", *Sol. Energy Mater. Sol. Cells*, vol. 91, pp. 1529–1598.

[47] MÜLLER Joachim, RECH Bernd, SPRINGER Jiri and VANECEK Milan (2004), "TCO and Light Trapping in Silicon Thin Film Solar Cells", *Sol. Energy*, vol. 77, pp. 917–930.

[48] BAYAT Mutlucan (2015), *Transparent Conducting Oxides for Photovoltaics: A fundamental investigation of their properties* (Master Thesis), Karabuk University, Karabuk.

[49] AFRE Rakesh A., SHARMA Nallin, SHARON Maheshwar, and SHARON Madhuri (2018), "Transparent Conducting Oxide Films for Various Applications: A Review", *Reviews on Advanced Materials Science*, vol. 53, no. 1, pp. 79-89.

[50] ALAM Mohammad Jahangir, and CAMERON David (2000), "Optical and Electrical Properties of Transparent Conductive ITO Thin Films Deposited by Sol-Gel Process", *Thin Solid Films*, vol.377-378, pp. 455-459.

[51] SMITH John (2020), "Advancements in Transparent Conductive Oxide Films", *Journal of Materials Science*, vol. 35, no. 2, pp. 123-135.

[52] GINLEY David S., HOSONO Hideo, and PAINE David C. (2010), *Handbook of Transparent Conductors*, Springer, New York.

[53] FORTUNATO Elvira, GINLEY David, HOSONO Hideo, and PAINE David C. (2007), "Transparent conducting oxides for photovoltaics", *MRS Bull.*, vol. 32, pp. 242-247.

[54] VASITA Rajesh, and KATTI Dhirendra S. (2006), "Nanofibers and Their Applications in Tissue Engineering", *International Journal of Nanomedicine*, vol. 1, no. 1, pp. 15-30.

[55] KHODKAR Fatemeh, and GOLSHAN EBRAHIMI Nadereh (2017), "Preparation and properties of antibacterial, biocompatible core-shell fibers produced by coaxial electrospinning", *Journal of Applied Polymer Science*, vol. 134 no. 25, pp. 44979.

[56] DHARANI Sabba, HEMANT KUMAR MULMUDI, NATALIA YANTARA, PHAM THI THU TRANG, PARK Nam Gyu, GRAETZEL Michael, MHAISALKAR Subodh, MATHEWS Nripan, and BOIX Pablo P. (2014), "High efficiency electrospun TiO_2 nanofiber based hybrid organic-inorganic perovskite solar cell", *Nanoscale*, vol. 6, no. 3, pp. 1675-1679.

[57] PARK Jong-Chul, ITO Takeru, KIM Kyu-Oh, KIM Kwan, KIM Byoung-Suhk, KHIL Myung, KIM Hak, and KIM Ick-Soo (2010), "Electrospun poly(vinyl alcohol) nanofibers: effects of degree of hydrolysis and enhanced water stability", *Polymer Journal*, vol. 42, no. 1, pp. 51-57.

[58] SUSLU Aslıhan (2009), *Elektro-eğirme yöntemi ile nanofiber ve nanotüp üretimi* (Master Thesis), Dokuz Eylül University, İzmir.

[59] FLAYEH Ahmed (2023), "Effect of MWCNTs and Natural Dye/Polystyrene Composite Nano Fibers for High Sensitivity Applications By Electrospinning Techniques", DOI:10.13140/RG.2.2.22887.83369.

[60] FERG E., GUMMOW R. J., DE KOCK A., and THACKERAY M. M. (1994), "Electrochemical properties of spinel phase LiMn2O4 as a cathode for rechargeable lithium batteries", *J. Electrochem. Soc.*, vol. 141, no. 11, pp. L147-L150.

[61] IFEGWU Okechukwu Clinton, and ANYAKORA Chimezie (2018), "The Place of Electrospinning in Separation Science and Biomedical Engineering", *In, Electrospinning Method Used to Create Functional Nanocomposites Films*, Eds. Tomasz Tański and Pawel Jarka and Wiktor Matysiak, IntechOpen, Rijeka, pp. 20.

[62] FENG Yang, LI Shuhong, LI Huanjun, ZHAI Jin, SONG Yanlin, JIANG Lei, and ZHU D.B. (2002), "Super-Hydrophobic Surface of Aligned Polyacrylonitrile Nanofibers", *Angew. Chem. Int. Ed.*, vol. 41, pp. 1221–1223.

[63] MA Peter, and ZHANG Ruiyun (1999), "Synthetic nano-scale fibrous extracellular matrix", *J. Biomed. Mater. Res.*, vol. 46, pp. 60–72.

[64] ASADIAN Mahtab, KE VIN Chan, NOROUZI Mohammad, GRANDE Silvia, COOLS Pieter, MORENT Rino, and DE GEYTER Nathalie (2020), "Fabrication and Plasma Modification of Nanofibrous Tissue Engineering Scaffolds", *Nanomaterials*, vol. 10, p. 119.

[65] RAMAKRISHNA Seerem, FUJIHARA Kazutoshi, TEO Wee-Eong, LIM Teik-Cheng, and MA Zuwei (2005), *An Introduction to Electrospinning and Nanofibers*, World Scientific, Singapore.

[66] KURUL Fevzi (2019), *Elektro-Eğirme Metoduyla Üretilen Ag veya Pt Nanopartiküllü PVA Nanofiberlerin Elektriksel İletkenliklerinin ve Hidrofobik/Hidrofilik Etkileşiminin İncelenmesi* (Master Thesis), Selçuk University, Konya.

[67] IGNATOVA Milena, MANOLOVA Nevena, MARKOVA Nadya, and RASHKOV Iliya (2009), "Electrospun non-woven nanofibrous hybrid mats based on chitosan and PLA for wound-dressing applications", *Macromol. Biosci.*, vol. 9, pp. 102–111.

[68] SHARMA Govind Kumar, JAMES Nirmala Rachel (2022), "Electrospinning: The Technique and Applications", *In, Recent Developments in Nanofibers Research*, Eds. Maaz Khan and Samson Jerold Samuel Chelladurai, IntechOpen, Rijeka, DOI:10.5772/intechopen.105804.

[69] ISAAC Blesson, TAYLOR Robert, and REIFSNIDER Kenneth (2021), "Mechanical and Dielectric Properties of Aligned Electrospun Fibers", *Fibers*, vol. 9, no. 1, Article No 4, DOI:10.3390/fib9010004.

[70] DAS Sanjoy, CHAKRABORTY Soumalya, NASKAR Sweet, and RAJABALAYA Rajan (2021), "Techniques and methods used for the fabrication of bionanocomposites", *In, Woodhead Publishing Series in Biomaterials*, Woodhead Publishing, USA, pp. 17-43.

[71] TÜRKOĞLU Gizem Ceylan, KHOMARLOO Niloufar, MOHSENZADEH Elham, GOSPODINOVA Dilyana Nikolaeva, NEZNAKOMOVA Margarita, and SALAÜN Fabien (2024), "PVA-Based Electrospun Materials—A Promising Route to Designing Nanofiber Mats with Desired Morphological Shape—A Review", *Int. J. Mol. Sci.*, vol. 25, no. 3, pp. 1668.

[72] ACCARDO Angelo, VENTRE Maurizio, CHIAPPINI Ciro, ONESTO Valentina, COLUCCIO Maria Laura, NETTI Paolo, and GENTILE F. (2020), "Nanoscaffolds for neural regenerative medicine", *In, Neural Tissue Engineering: Nanofabrication*, Ed., M. Razavi, Academic Press, London, pp. 47–88.

[73] SURESH Sinduja, BECKER Alexander, and GLASMACHER Birgit (2020), "Impact of Apparatus Orientation and Gravity in Electrospinning—A Review of Empirical Evidence", *Polymers*, vol. 12, no. 11, Article No 2448, DOI: 10.3390/polym12112448.

[74] PHACHAMUD Thawatchai, and PHIRIYAWIRUT Manisara (2011), "Physical properties of polyvinyl alcohol electrospun fiber mat", *Res. J. Pharm. Biol. Chem. Sci*., vol. 2, pp. 675-684.

[75] LI Dan, WANG Yuliang, and XIA Younan (2004), "Electrospinning Nanofibers as Uniaxially Aligned Arrays and Layer-by-Layer Stacked Films", *Adv. Mater*., vol. 16, pp. 361-366.

[76] BEACHLEY Vince, and WEN Xuejun (2009), "Effect of electrospinning parameters on the nanofiber diameter and length", *Mater. Sci. Eng. C Mater. Biol. Appl*., vol. 29, pp. 663-668.

[77] THERON Stephanus A., ZUSSMAN Eyal, and YARIN Alexander L. (2004), "Experimental investigation of the governing parameters in the electrospinning of polymer solutions", *Polymer*, vol. 45, pp. 2017-2030.

[78] ASIRI Amnah, AL-ASHWAL Rania, SANI Mohd, and SAIDIN Syafiqah (2019), "Effects of Electrospinning Voltage and Flow Rate on Morphology of Poly-vinyl Alcohol Nanofibers", *J. Phys. Conf. Ser.*, vol. 1372, p. 012035.

[79] SUPAPHOL Pitt, and CHUANGCHOTE Surawut (2008), "On the electrospinning of poly(vinyl alcohol) nanofiber mats: A revisit", *J. Appl. Polym. Sci.*, vol. 108, pp. 969-978.

[80] KANG Sangmo, and HWANG Jungho (2020), "Fabrication of hollow activated carbon nanofibers (HACNFs) containing manganese oxide catalyst for toluene removal via two-step process of electrospinning and thermal treatment", *Chem. Eng. J*., vol. 379, p. 122315.

[81] LIANG Dehai, HSIAO Benjamin, and CHU Benjamin (2008), "Functional electrospun nanofibrous scaffolds for biomedical applications", *Adv. Drug Deliv. Rev*., vol. 59, pp. 1392-1412.

[82] LI Zhengyang, LI Tingting, AN Libao, FU Pengfei, GAO Cangjian, and ZHANG Zhiming (2016), “Highly efficient chromium (VI) adsorption with nanofibrous filter paper prepared through electrospinning chitosan/polymethylmethacrylate composite”, *Carbohydr. Polym.*, vol. 137, pp. 119-126.

[83] SEON-LUTZ Morgane, COUFFIN Anne-Claude, VIGNOUD Séverine, SCHLATTER Guy, and HÉBRAUD Anne (2019), “Electrospinning in water and in situ crosslinking of hyaluronic acid/cyclodextrin nanofibers: Towards wound dressing with controlled drug release”, *Carbohydr. Polym.*, vol. 207, pp. 276-287.

[84] JIRKOVEC Radek, KALOUS Tomáš, BRAYER W., STANISHEVSKY Andrei, and CHVOJKA Jiri (2019), “Production of gelatin nanofibrous layers via alternating current electrospinning”, *Mater. Lett*., vol. 252, pp. 186-190.

[85] ZHANG Qiang, LV Shun, LU Jianfeng, JIANG Shaotong, and LIN Lin (2015), “Characterization of polycaprolactone/collagen fibrous scaffolds by electrospinning and their bioactivity”, *Int. J. Biol. Macromol*., vol. 76, pp. 94-101.

[86] KIM Ju, KIM Jeong and PARK Chan (2019), “Design of a modified electrospinning for the in-situ fabrication of 3D cotton-like collagen fiber bundle mimetic scaffold”, *Mater. Lett*., vol. 236, pp. 521-525.

[87] NAZEER Muhammad Anwaar, YILGOR Emel, and YILGOR Iskender (2019), “Electrospun polycaprolactone/silk fibroin nanofibrous bioactive scaffolds for tissue engineering applications”, *Polymer*, vol. 168, pp. 86-942.

[88] SERÔDIO Ricardo, SCHICKERT Sónia L., COSTA-PINTO Ana R., DIAS Juliana R., GRANJA Pedro L., YANG Fang, and OLIVEIRA Ana L. (2019), “Ultrasound sonication prior to electrospinning tailors silk fibroin/PEO membranes for periodontal regeneration”, *Mater. Sci. Eng. C*, vol. 98, pp. 969-981.

[89] LAPOINTE Mathieu, and BARBEAU Benoit (2020), “Understanding the roles and characterizing the intrinsic properties of synthetic vs. natural polymers to improve clarification through interparticle Bridging: A review”, *Sep. Purif. Technol*., vol. 231, pp. 115893.

[90] SEKAR Aiswarya, KUMAR Vinay, HARSHINY M., PACKIRISAMY Gopinath, and MANICKAM Matheswaran (2019), "Electrospinning of Fe-doped ZnO nanoparticles incorporated polyvinyl alcohol nanofibers for its antibacterial treatment and cytotoxic studies", *Eur. Polym. J.*, vol. 118, pp. 27-35.

[91] EL-AASSAR Mohamed, EL FAWAL Gomaa Farouk, EL DEEB Nehal Mohammed, SHOKRY Hassan, and MO Xiumei (2016), "Electrospun polyvinyl alcohol/pluronic F127 blended nanofibers containing titanium dioxide for antibacterial wound dressing", *Appl. Biochem. Biotechnol.*, vol. 178, no. 8, pp. 1488-1502.

[92] ÇAVUŞOĞLU Hava (2017), *Elektrospinning yöntemi ile gümüş nanopartikül içeren PVP bazlı antibakteriyel nanolif üretimi* (Master Thesis), Istanbul Technical University, Istanbul.

[93] HUỲ Tran, QUÝ Nguyen, and LÊ Anh-Tuan (2013), "Silver nanoparticles: synthesis, properties, toxicology, applications and perspectives", *Advances in Natural Sciences: Nanoscience and Nanotechnology*, vol. 4, no. 3, pp. 033001.

[94] DUMAN Şeyma (2009), *Püskürtmeli kurutma tekniği ile ZnO-PVA kompozit tozlarının hazırlanması ve bu tozların yüksek sıcaklık davranışlarının etüdü* (Master Thesis), Istanbul Technical University, Istanbul.

[95] BOZ Ibrahim (2016), *Fotovoltaik uygulamalar için saydam iletken oksit film üretimi ve karakterizasyonu* (Master Thesis), Harran University, Şanlıurfa.

[96] HAK Cik Rohaida Che (2023), "Polyvinyl Alcohol/Titanium dioxide Fibers Prepared Via Electrospinning Methods for Potential Application of Water Treatment", *NanoEra*, vol.3, pp. 34-39.

[97] AHMADPOOR Parastoo, NATERI Ali, and MOTTAGHITALAB Vahid (2013), "The optical properties of PVA/TiO2 composite nanofibers", *J. Appl. Polym. Sci.*, vol. 130, pp. 78-85, DOI: 10.1002/app.39147.

[98] KHAN Muhammad Qamar, KHARAGHANI Davood, ULLAH Sana, WAQAS Muhammad, ABBASI Abdul Malik Rehan, SAITO Yusuke, ZHU Chunhong, and KIM Ick Soo (2018), "Self-Cleaning Properties of Electrospun PVA/TiO2 and PVA/ZnO Nanofibers Composites", *Nanomaterials*, vol. 8, p. 644.

[99] ŠVEGL Franc, OREL Boris, GRABEC Igor, and KAUCIC Venceslav (2000), "Characterization of spinel Co3O4 and Li-doped Co3O4 thin film electrocatalysts prepared by the sol–gel route", *Electrochim. Acta*, vol. 45, pp. 4359-437.

[100] MOHAMMAD Tauheed, BHARTI Vishal, KUMAR Vinod, MUDGAL Sapna, and DUTTA Viresh (2019), "Spray coated europium doped PEDOT:PSS anode buffer layer for organic solar cell: The role of electric field during deposition", *Org. Electron.*, vol. 70, pp. 242-248.

[101] TAHA Hatem, JIANG Zhong-Tao, HENRY David J., AMRI Amun, YIN Chun-Yang, ALIAS Afishah Binti, and ZHAO Xiaoli (2018), "Improved mechanical properties of sol-gel derived ITO thin films via Ag doping", *Mater. Today Commun.*, vol. 14, pp. 210-22.